Lecture Notes in Electrical Engineering 390

Jiadong Sun
Jingnan Liu
Shiwei Fan
Feixue Wang
Editors

China Satellite Navigation Conference (CSNC) 2016 Proceedings: Volume III

Springer

Lecture Notes in Electrical Engineering

Volume 390

About this Series

"Lecture Notes in Electrical Engineering (LNEE)" is a book series which reports the latest research and developments in Electrical Engineering, namely:

- Communication, Networks, and Information Theory
- Computer Engineering
- Signal, Image, Speech and Information Processing
- Circuits and Systems
- Bioengineering

LNEE publishes authored monographs and contributed volumes which present cutting edge research information as well as new perspectives on classical fields, while maintaining Springer's high standards of academic excellence. Also considered for publication are lecture materials, proceedings, and other related materials of exceptionally high quality and interest. The subject matter should be original and timely, reporting the latest research and developments in all areas of electrical engineering.

The audience for the books in LNEE consists of advanced level students, researchers, and industry professionals working at the forefront of their fields. Much like Springer's other Lecture Notes series, LNEE will be distributed through Springer's print and electronic publishing channels.

More information about this series at http://www.springer.com/series/7818

Jiadong Sun · Jingnan Liu
Shiwei Fan · Feixue Wang
Editors

China Satellite Navigation Conference (CSNC) 2016 Proceedings: Volume III

Springer

Editors
Jiadong Sun
Chinese Academy of Sciences
China Aerospace Science and Technology Corporation
Beijing
China

Jingnan Liu
Wuhan University
Wuhan
China

Shiwei Fan
China Satellite Navigation Office
Beijing
China

Feixue Wang
National University of Defense Technology
Changsha
China

ISSN 1876-1100 ISSN 1876-1119 (electronic)
Lecture Notes in Electrical Engineering
ISBN 978-981-10-0939-6 ISBN 978-981-10-0940-2 (eBook)
DOI 10.1007/978-981-10-0940-2

Library of Congress Control Number: 2016937343

Printed on acid-free paper

This Springer imprint is published by Springer Nature
The registered company is Springer Science+Business Media Singapore Pte Ltd.

Preface

BeiDou Navigation Satellite System (BDS) is China's global navigation satellite system which has been developed independently. BDS is similar in principle to global positioning system (GPS) and compatible with other global satellite navigation systems (GNSS) worldwide. The BDS will provide highly reliable and precise positioning, navigation and timing (PNT) services as well as short-message communication for all users under all-weather, all-time, and worldwide conditions.

China Satellite Navigation Conference (CSNC) is an open platform for academic exchanges in the field of satellite navigation. It aims to encourage technological innovation, accelerate GNSS engineering, and boost the development of the satellite navigation industry in China and in the world.

The 7th China Satellite Navigation Conference (CSNC2016) is held during May 18–20, 2016, Changsha, China. The theme of CSNC2016 is Smart Sensing, Smart Perception, including technical seminars, academic exchanges, forums, exhibitions, and lectures. The main topics are as follows:

S1 BDS/GNSS Application Technology
S2 Navigation and Location Based Services
S3 Satellite Navigation Signals
S4 Satellite Orbit and Clock Offset Determination
S5 BDS/GNSS Precise Positioning Technology
S6 Atomic Clock and Time-frequency Technology
S7 BDS/GNSS Augmentation Systems and Technology
S8 BDS/GNSS Test and Assessment Technology
S9 BDS/GNSS User Terminal Technology
S10 Multi-sensor Fusion Navigation
S11 PNT System and Emerging Navigation Technology
S12 Standardization, Intellectual Properties, Policies, and Regulations

The proceedings (Lecture Notes in Electrical Engineering) have 176 papers in ten topics of the conference, which were selected through a strict peer-review process from 440 papers presented at CSNC2016. In addition, another 193 papers

were selected as the electronic proceedings of CSNC2016, which are also indexed by "China Proceedings of Conferences Full-text Database (CPCD)" of CNKI and Wan Fang Data.

We thank the contribution of each author and extend our gratitude to 237 referees and 48 session chairmen who are listed as members of editorial board. The assistance of CNSC2016's organizing committees and the Springer editorial office is highly appreciated.

The 7th China Satellite Navigation Conference (CSNC 2016) Committees

Scientific Committee

Chairman
Jiadong Sun, China Aerospace Science and Technology Corporation

Vice-Chairman
Rongjun Shen, China
Jisheng Li, China
Qisheng Sui, China
Changfei Yang, China
Zuhong Li, China Academy of Space Technology
Shusen Tan, Beijing Satellite Navigation Center, China

Executive Chairman
Jingnan Liu, Wuhan University
Yuanxi Yang, China National Administration of GNSS and Applications
Shiwei Fan, China

Committee Members (By Surnames Stroke Order)
Xiancheng Ding, China Electronics Technology Group Corporation
Qingjun Bu, China
Liheng Wang, China Aerospace Science and Technology Corporation
Yuzhu Wang, Shanghai Institute of Optics and Fine Mechanics, Chinese Academy of Sciences
Guoxiang Ai, National Astronomical Observatories, Chinese Academy of Sciences
Shuhua Ye, Shanghai Astronomical Observatories, Chinese Academy of Sciences
Zhaowen Zhuang, National University of Defense Technology
Qifeng Xu, PLA Information Engineering University
Houze Xu, Institute of Geodesy and Geophysics, Chinese Academy of Sciences
Guirong Min, China Academy of Space Technology

Xixiang Zhang, China Electronics Technology Group Corporation
Lvqian Zhang, China Aerospace Science and Technology Corporation
Junyong Chen, National Administration of Surveying, Mapping and Geoinformation
Benyao Fan, China Academy of Space Technology
Dongjin Luo, China
Guohong Xia, China Aerospace Science and Industry Corporation
Chong Cao, China Research Institute of Radio Wave Propagation (CETC 22)
Faren Qi, China Academy of Space Technology
Sili Liang, China Aerospace Science and Technology Corporation
Shancheng Tu, China Academy of Space Technology
Rongsheng Su, China
Zhipeng Tong, China Electronics Technology Group Corporation
Ziqing Wei, Xi'an Institute of Surveying and Mapping

Organizing Committee

Secretary General
Haitao Wu, Navigation Headquarters, Chinese Academy of Sciences

Vice Secretary General
Wenhai Jiao, China Satellite Navigation Office Engineering Center
Jianjun Wu, National University of Defense Technology
Weina Hao, Navigation Headquarters, Chinese Academy of Sciences

Committee Members (By Surnames Stroke Order)
Qun Ding, The 20th Research Institute of China Electronics Technology Group Corporation
Miao Yu, China Academy of Space Technology
Li Wang, International Cooperation Research Center China Satellite Navigation Engineering Office
Ying Liu, China Satellite Navigation Office Engineering Center
Shuhua Zhang, National University of Defense Technology, Changsha
Xiuwan Chen, Peking University
Xiangan Zhao, China Defense Science and Technology Information Center
Ouyang Guangzhou, Academy of Opto-electronics, Chinese Academy of Sciences
Gang Hu, Beijing Unicore Communications, Inc.
Min Shui, National Remote Sensing Centre of China
Zhong Dou, National Time Service Center, Chinese Academy of Sciences

Editorial Board

Topic S5: BDS/GNSS Precise Positioning Technology
BDS/GNSS Precise Positioning Technology
Qile Zhao, Wuhan University
Jianwen Li, Information Engineering University
Song shuLi, Shanghai Astronomical Observatory, Chinese Academy of Sciences
Yanming Feng, Queensland University of Technology, Brisbane, Australia

Topic S6: Atomic Clock and Time-frequency Technology
Lianshan Gao, The 203th Research Institute of China Aerospace Science and Industry Corporation
Chunhao Han, Beijing Satellite Navigation Center
Xiaohui Li, National Time Service Center, Chinese Academy of Sciences
Nikolay Demidov, VCH Corporation, Russia

Topic S7: BDS/GNSS Augmentation Systems and Technology
Junlin Zhang, OLinkStar Co., Ltd., China
Jinping Chen, Beijing Satellite Navigation Center
Rui Li, Beihang University
Shaojun Feng, Imperial College London

Topic S8: BDS/GNSS Test and Assessment Technology
Jun Yang, National University of Defense Technology
Xiaolin Jia, Xi'an Institute of Surveying and Mapping
Wenxian Yu, Shanghai Jiao Tong University
Yang Gao, University of Calgary, Canada

Topic S9: BDS/GNSS User Terminal Technology
Haibo He, Beijing Satellite Navigation Center
Baowang Lian, Northwestern Polytechnical University
Hong Li, Tsinghua University
Yong Li, University of New South Wales, Australia

Topic S10: Multi-sensor Fusion Navigation
Zhongliang Deng, Beijing University of Posts and Telecommunications
Hong Yuan, Academy of Opto-electronics, Chinese Academy of Sciences
Yongbin Zhou, National University of Defense Technology
Jinling Wang, University of New South Wales, Australia

Topic S11: PNT System and Emerging Navigation Technology
Mingquan Lu, Tsinghua University
Wei Wang, The 20th Research Institute of China Electronics Technology Group Corporation
Yin Xu, Academy of Opto-electronics, Chinese Academy of Sciences
Xiangzhen Li, Chungnam National University, Korea

Topic S12: Standardization, Intellectual Properties, Policies, and Regulations
Daiping Zhang, China Defense Science and Technology Information Center
Yonggang Wei, China Academy of Aerospace Standardization and Product Assurance
Haibo Liu, Institute of Policy and Management, Chinese Academy of Sciences
Haibo Wang, Electronic Intellectual Property Center, Ministry of Industry and Information Technology, PRC

Contents

Part I
Satellite Orbit and Clock Offset Determination

Research on the Inversion Method of USO Frequency Stability Joining GNSS and Inter-satellite Distance Measurement

Xuan Liu, Dengfeng Wang, Xingwang Zhong and Yansong Meng

Abstract K-band ranging (KBR) system and GNSS receiver are the key payloads of the gravity exploration satellite which employs LEO satellite tracking LEO satellite technology. Ultra-stable crystal oscillator, providing precise inter-satellite distance measurement with clock frequency reference, is the key component of the KBR-GNSS system. Therefore, real-time and dynamic monitoring on-orbit ultra-stable oscillator (USO)'s frequency stability are very necessary. First of all, the analysis formula of DOWR with time-tag corrected is deduced based on the study of the KBR-GNSS measuring principle. Second, the coupling relationship between Allan variance formula and inter-satellite time difference is analyzed deeply. Two methods of inversing USO Allan variance are proposed, of which one is using inter-satellite time difference measurement and the other one is employing inter-satellite distance measurement. Finally, referring to GRACE satellite payload scheme, a set of KBR-GNSS system is developed, by using which, the effectiveness of the two algorithms is validated and their advantages and disadvantages are compared meanwhile. The research results of this paper have some references to the design of inter-satellite ranging system of Chinese first generation earth gravity exploration satellite.

Keywords GNSS K-band ranging · Dual one-way ranging · Ultra-stable oscillator Allan variance · Gravity field exploration

X. Liu (✉) · D. Wang · X. Zhong · Y. Meng
China Academy of Space Technology, No. 504 Chang'an Eastern Street, Xi'an, China
e-mail: liuxuan0229@126.com

D. Wang
e-mail: wangdf79@163.com

X. Zhong
e-mail: zhongxw1391@qq.com

Y. Meng
e-mail: yansongmeng@hotmail.com

J. Sun et al. (eds.), *China Satellite Navigation Conference (CSNC) 2016 Proceedings: Volume III*, Lecture Notes in Electrical Engineering 390,
DOI 10.1007/978-981-10-0940-2_1

1 Introduction

The precise measurement of the earth's gravity field shows great application value in oceanography, hydrology, geophysical science, and military aspects. Leo satellite tracking Leo satellite technology, referred to as SST-LL, is one of the most effective means of detection of gravitational field [1]. GRACE (Gravity Recovery and Climate Experiment) satellite jointly developed by The United States and Germany was launched in 2002, in which SST-LL technology was used for the first time. High precision K-band ranging (KBR) and GNSS receiver are the core payloads of the GRACE, of which ultra-stable oscillator (USO) is the key equipment. USO is the standard of time and frequency of KBR and GNSS receiver in which all of the measuring time tags are referenced to USO's output. During on-orbit operation process, USO is influenced by various factors such as temperature, radiation, and aging so that its frequency is not stable, thereby affecting measurement accuracy of KBR and GNSS receiver [2]. Consequently, monitoring of on-orbit USO frequency stability for measurement data processing and analysis are of great help.

China has launched the earth's gravity field exploration program. Related research institutions and scholars have made deep study in KBR, USO, and GNSS receiver [3, 4]. Taking GRACE satellites as the background, based on the principles of two one-way ranging (DOWR) and high precision time difference correction, combining with the self-developed KBR-GNSS experimental systems, this paper intensively studies the indirect calculation method of USO frequency stability. Starting from the original definition of Allan variance, the relative Allan variance mathematical model is firstly proposed by inter-satellites time difference value and then further established using biased distance between satellites. Direct measurement and indirect computing results of USO Allan variance are compared and analyzed, which verifies the accuracy and feasibility of indirect calculation methods. Finally, some suggestions and considerations are put forward to Chinese earth's gravity field exploration satellites.

2 Principle of Measurement

2.1 Dual One-Way Ranging

As showed in Fig. 1, satellite i and satellite j transmit Ka band signal to each other, respectively, and the difference of these signals is 670 kHz. The receiving terminals uninterruptedly monitor the phase changes of 670 kHz signal using phase locked loop to obtain one-way phase measurements φ_i^j and φ_j^i.

The theoretical basis of KBR is DOWR which can effectively suppress the common error caused by medium and long term frequency instability of USO [4], as showed in Fig. 2. At the specified nominal measuring time t, the one-way phase measurement of satellite i can be expressed as [5]:

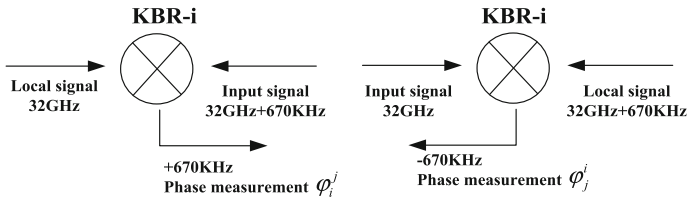

Fig. 1 KBR signal flow graph

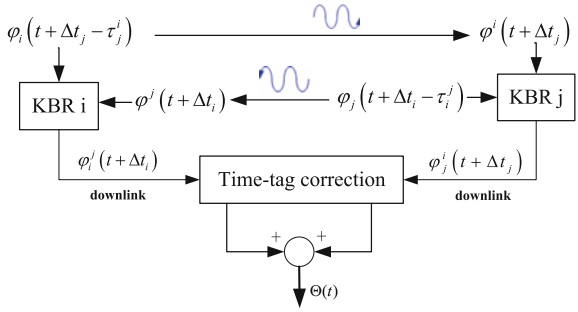

Fig. 2 Schematic of dual one-way phase measurement

$$\varphi_i^j(t+\Delta t_i)=\varphi_i(t+\Delta t_i)-\varphi^j(t+\Delta t_i)+E_i^j \quad i,j=1,2,\ \ i\neq j \tag{1}$$

Formula (1) is the phase difference from the received signal and the local reference signal, among which the phase of received signal in satellite i can be represented by the one of transmitted signal in satellite j.

$$\varphi^j(t+\Delta t_i)=\varphi_j\left(t+\Delta t_i-\tau_i^j\right) \tag{2}$$

where τ_i^j is the signal travel time from satellite j to i. So, formula (1) can be written as:

$$\varphi_i^j(t+\Delta t_i)=\varphi_i(t+\Delta t_i)-\varphi_j\left(t+\Delta t_i-\tau_i^j\right)+E_i^j \tag{3}$$

Δt_i called time-tag error is the difference of actual and nominal sampling time, which needs to be corrected by GNSS measurement. E_i^j is the sum of measurement errors including integer ambiguity, ionosphere error, and other phase measuring errors.

Phase $\varphi_i(t)$ can be decomposed into the reference phase $\bar{\varphi}_i$ and phase errors caused by the oscillator $\delta\varphi_i$

$$\varphi_i(t) = \bar{\varphi}_i(t) + \delta\varphi_i(t) \tag{4}$$

So, formula (3) can be written as:

$$\begin{aligned}\varphi_i^j(t+\Delta t_i) = {} & \bar{\varphi}_i(t+\Delta t_i) + \delta\varphi_i(t+\Delta t_i) \\ & - \bar{\varphi}_j(t+\Delta t_i - \tau_i^j) - \delta\varphi_j(t+\Delta t_i - \tau_i^j) + E_i^j\end{aligned} \tag{5}$$

Formula (5) can be arranged using Taylor polynomial method, in which phase change $\dot{\bar{\varphi}}_i(t)$ is represented by constant standard frequency f_i. Then following four expressions can be obtained:

$$\begin{aligned}\bar{\varphi}_i(t+\Delta t_i) &\approx \bar{\varphi}_i(t) + \dot{\bar{\varphi}}_i(t)\Delta t_i \approx \bar{\varphi}_i(t) + f_i\Delta t_i \\ \bar{\varphi}_i(t+\Delta t_j - \tau_j^i) &\approx \bar{\varphi}_i(t) + f_i\Delta t_j - f_i\tau_j^i \\ \delta\varphi_i(t+\Delta t_i) &\approx \delta\varphi_i(t) + \delta f_i(t)\Delta t_i \\ \delta\varphi_i(t+\Delta t_i - \tau_j^i) &\approx \delta\varphi_i(t) + \delta f_i(t)\Delta t_i - \delta f_i(t)\tau_j^i\end{aligned} \tag{6}$$

In that way, the result of DOWR is [5]:

$$\Theta \equiv \varphi_i^j(t+\Delta t_i) + \varphi_j^i(t+\Delta t_j) \tag{7}$$

Because the frequencies of microwave signal in two satellites are designed differently, f_1 represents the microwave signal in satellite i while f_2 represents that in satellite j. If formula (6) is substituted into (5) and then formula (5) is substituted into (7), it can be got that:

$$\begin{aligned}\Theta(t) \approx {} & (f_i\tau_j^i + f_j\tau_i^j) + (\delta f_i\tau_j^i + \delta f_j\tau_i^j) \\ & + (f_i - f_j)(\Delta t_i - \Delta t_j) + (\delta f_i - \delta f_j)(\Delta t_i - \Delta t_j) + E\end{aligned} \tag{8}$$

Consequently, the biased distance measurement can be written as:

$$R(t) = \lambda\Theta(t), \quad \lambda = c/(f_i + f_j) \tag{9}$$

2.2 Time-Tag Correction DOWR

As mentioned before that DOWR can effectively suppress the phase errors caused by medium and long term frequency instability of USO, a key prerequisite of ensuring noise suppression ratio is that measurement time consistency must reach a certain precision when two one-way phase measurements are superimposed based on Eq. (7). GRACE requires that this time consistency is better than 0.1 ns. In practical projects, it can be ensured that the GNSS pseudorange measurements are

tagged with KBR measuring time if the time-tag produced by local USO is used to sample GNSS and KBR measurements at the same time. In this paper, GNSS and KBR measuring time are denoted by t_i^{gnss} and t_i, respectively.

$$\begin{aligned}\Delta t &= \Delta t_i - \Delta t_j = (t_i - t_{\text{gnss}}) - (t_j - t_{\text{gnss}}) \\ &= (t_i^{\text{gnss}} - t_{\text{gnss}}) - (t_j^{\text{gnss}} - t_{\text{gnss}}) = t_i^{\text{gnss}} - t_j^{\text{gnss}}\end{aligned} \tag{10}$$

As showed in Fig. 2, Δt is used to correct KBR measuring time and two one-way phase measurements from satellite i and satellite j can be resampled at nearly the same time. In practice, it is chosen that measurement of satellite j is resampled at t_i. Where Δt, got through GNSS data post-processing, is used to interpolate one-way phase measurement of satellite j, which is showed in the following expression

$$\begin{aligned}\varphi_j^i(t+\Delta t_j) &= \varphi_j^i(t+\Delta t_i - \Delta t) \\ &= \bar{\varphi}_j(t+\Delta t_i - \Delta t) + \delta\varphi_j(t+\Delta t_i - \Delta t) \\ &\quad - \bar{\varphi}_j(t+\Delta t_i - \Delta t - \tau_j^i) - \delta\varphi_j(t+\Delta t_i - \Delta t - \tau_j^i) + E_j^i\end{aligned} \tag{11}$$

Until now, the equation of DOWR is rewritten after time-tag correction as:

$$\begin{aligned}\Theta(t_i) \approx\ & (f_i\tau_j^i + f_j\tau_i^j) + (\delta f_i\tau_j^i + \delta f_j\tau_i^j) \\ & + (f_i - f_j)\delta|\Delta t_i| + (\delta\dot{\varphi}_i - \delta\dot{\varphi}_j)\delta\left|\Delta t_j\right| + E\end{aligned} \tag{12}$$

where $\delta|\Delta t_i|$ and $\delta\left|\Delta t_j\right|$ are time difference measuring errors which are very small and can be neglected [6] (Fig. 3).

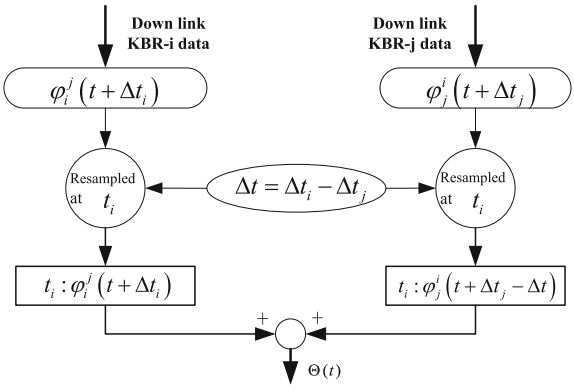

Fig. 3 Principle of time-tag correction

2.3 Relative Frequency Error

Formula (12) subtracts formula (8), neglecting the small terms:

$$\Theta(t_i) - \Theta(t) \approx (f_i - f_j)(\Delta t_i - \Delta t_j) + (\delta f_i - \delta f_j)(\Delta t_i - \Delta t_j) \tag{13}$$

Defining a new composite phase measurement as:

$$\Theta_p(t) = \Theta(t) - (f_i - f_j)(\Delta t_i - \Delta t_j) \tag{14}$$

Formula (15) can be got if formula (14) subtracts formula (12):

$$\Theta_p(t) - \Theta(t_i) \approx (\delta f_i - \delta f_j)(\Delta t_i - \Delta t_j) \tag{15}$$

As a result, relative frequency error is:

$$\delta f_i - \delta f_j \approx \frac{\Theta_p(t) - \Theta(t_i)}{\Delta t_i - \Delta t_j} \tag{16}$$

2.4 Relative Allan Variance

The so-called frequency stability is the degree of any frequency source producing the same frequency in a period after continuous operation for a while, also described as the degree of frequency random fluctuation. The frequency instability, in time domain, is generally characterized by Allan variance. Any oscillator can output a signal that can be described as the following formula:

$$A(t) = [A + \varepsilon(t)] \sin[2\pi f_0 t + \varphi(t)] \tag{17}$$

A is the amplitude and f_0 is the nominal frequency. $\varepsilon(t)$ and $\varphi(t)$ represent the random amplitude and phase fluctuations with respect to the ideal case. Then, phase deviation can be expressed as [7]:

$$x(t) = \varphi(t)/2\pi f_0 \tag{18}$$

$$y(t) = \dot{\varphi}(t)/2\pi f_0 \tag{19}$$

where $\dot{\varphi}(t) = \delta f_i - \delta f_j$, δf_i is frequency error. Formula (18) signifies relative time deviation and formula (19) signifies relative frequency deviation. As a result, Allan variance is defined as:

$$\sigma(\tau) = \left[\frac{1}{2(N-1)}\sum_{i=1}^{N-1}(y_{i+1} - y_i)^2\right]^{1/2} \tag{20}$$

where $y_n = (x_n - x_{n-1})/\tau$ represents the average frequency deviation of Nth interval. So, Allan variance can be rewritten as:

$$\sigma_x(\tau) = \left[\frac{1}{2(N-1)\tau^2}\sum_{i=1}^{N-1}(x_{i+2} - 2x_{i+1} + x_i)^2\right]^{1/2} \tag{21}$$

If $x = \Delta t$, relative Allan variance can be got:

$$\sigma_{\Delta t}(\tau) = \left[\frac{1}{2(N-1)\tau^2}\sum_{i=1}^{N-1}(\Delta t_{i+2} - 2\Delta t_{i+1} + \Delta t_i)^2\right]^{1/2} \tag{22}$$

A new relative frequency deviation expression can be got if substituting formula (16)–(19):

$$\bar{y} = \frac{\delta f_i - \delta f_j}{(f_i + f_j)/2} \tag{23}$$

δf_i and δf_j represent the deviation with respect to the nominal frequency of USO in satellite i and satellite j, respectively. $(f_i + f_j)/2$ signifies average nominal frequency. On these basis, corrected Allan variance based on KBR measurement can be expressed as:

$$\sigma_{\bar{y}}(\tau) = \left[\frac{1}{2(N-1)}\sum_{i=1}^{N-1}(\bar{y}_{i+1} - \bar{y}_i)^2\right]^{1/2} \tag{24}$$

In the end, for computing two USOs' relative Allan variance, the Eq. (22) based on inter-satellites time difference measurement and Eq. (24) based on GNSS and KBR measurements are obtained. What needs to be pointed out is that Allan variance getting from these equations represents the overall level of the two USOs' frequency stability. Given two USOs are running independently in two satellites, it can be estimated that Allan variance of single USO is about half of the two USOs' relative Allan variance.

3 Test and Verification

3.1 Testing System

As shown in Fig. 4, two sets of KBR-GNSS experimental system referenced to GRACE KBR were self-developed and a ground test system was build accordingly. KBR-GNSS system consists of K band and L band antenna, RF transceiver that is used for up-conversion and down-conversion reference signal, USO which produces local reference frequency and digital signal processing unit which handles GNSS signal processing and KBR carrier phase extraction. All the tests were carried out in a special anechoic chamber in order to restrain multipath signal, in which free signal propagation distance was about 3.5 m. Only 32 GHz microwave was used because the ground test did not involve the ionosphere calibration. Digital signal processing unit obtains one-way phase measurements for KBR on one hand and tracks GNSS navigation signal, generating pseudorange measurements. Then packaged KBR and GNSS measurements are sent to special testing equipment. After data preprocessing, precision time-tag acquisition and DOWR arrangement, biased distance and time difference value between the satellites are, respectively, got.

3.2 Testing Results

A lot of KBR and GNSS observations were got under the help of the testing system with the almost constant temperature and pressure environment. Testing results showed that the precision of the measuring time difference values of two KBR got from GNSS data was up to 0.1 ns and KBR biased distance precision using time-tag correction DOWR was better than 10 μm as shown in Fig. 5.

After dealing with the same set of test data using Eq. (22) with (24), respectively, the average frequency stability of individual USO was estimated accordingly. In order to reduce one-way KBR errors apart from error sources caused by

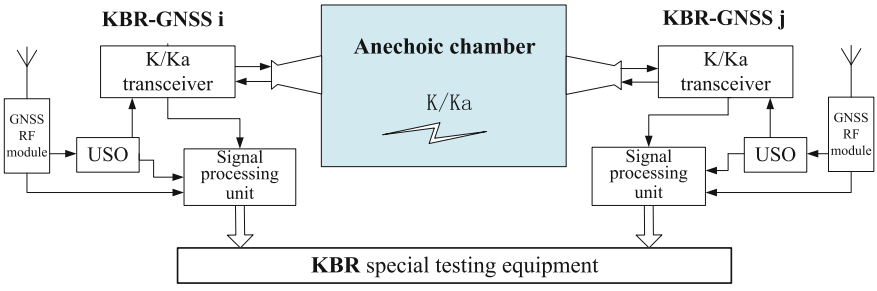

Fig. 4 Experimental system of SST-LL KBR-GNSS

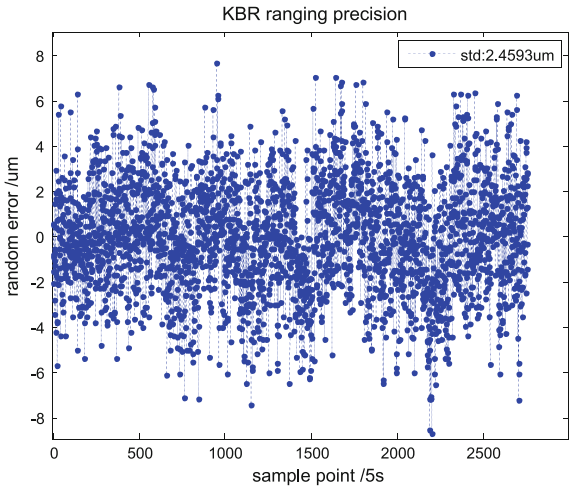

Fig. 5 KBR range error time series

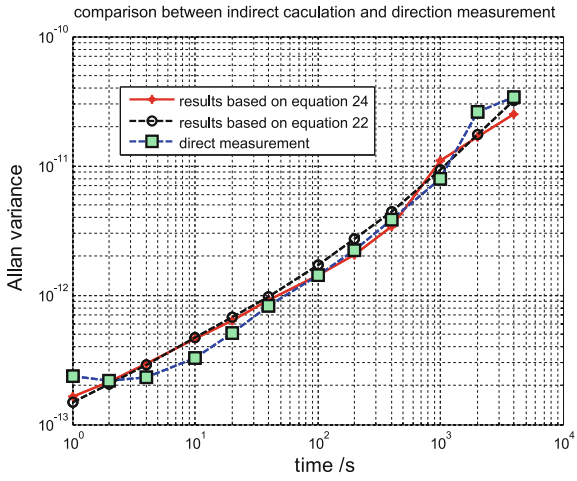

Fig. 6 Allan variance results of indirect calculation and direct measurement

USO frequency instability as much as possible, several tests kept two KBR-GNSS systems relatively static, the receiver carrier to noise ratio consistent and environment temperature basic constant, so that the multipath error, system noise and ranging system error were kept within the reasonable scope, which was advantageous to accurately assessing the validity of the indirect frequency stability calculation method.

For the same set of test data, Fig. 6 shows the individual USO Allan variance estimation curve using two calculation methods and measured curve by TSC5115A cooperated with OSA8607D (10 MHz) for comparison. Allan variance based on time-tag difference is got by Eq. (22), while Allan variance based on distance and time-tag joint model is obtained by Eq. (24). Direct measurement curve is the

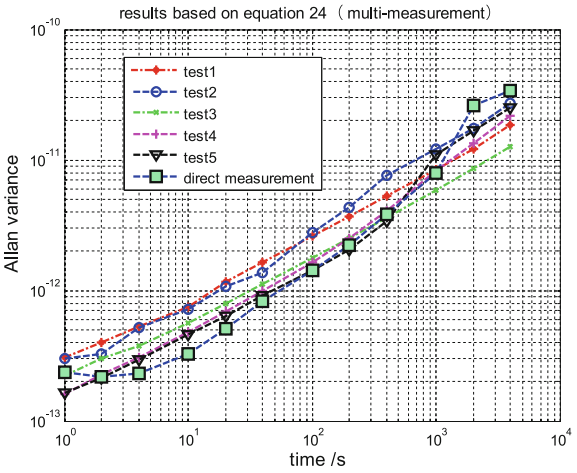

Fig. 7 Allan variance computing results based on the joint model Eq. (24)

average of the two USO Allan variance using TSC5115A. Figure 6 shows that the results of two indirect calculation methods are in good consistency and are consistent with the direct measured results.

Figure 7 shows the Allan variance based on Eq. (24) using five different sets of test data, in which the trend of five indirect calculation results are almost consistent with slightly difference at the same time point and the average of indirect results is higher than direct measurements at the same time point.

However, RF transceiver and USO are very sensitive to tiny changes in temperature. Thus, the instability of temperature difference of two KBRs might introduce offset in phase measurement. In addition, multipath signal and small ground vibration also had influence on the phase measurement. All these factors mentioned above were eventually transformed into phase measurement noise of the short and medium term of KBR, and then influenced Allan variance calculation results. That is why five indirect calculation results in Fig. 7 are not in full accord.

4 Conclusion

The formula of indirectly calculating relative frequency error of two USOs based on KBR phase measurement was deduced, and then the equation of relative Allan variance based on relative frequency error and relative time difference were obtained, respectively. USO Allan variance was estimated indirectly using KBR and GNSS data based on two methods and measured directly using standard instrument. The results of these two ways were compared, showing that the results were basically identical. If a single comparison was made to two kinds of calculation methods, it could be seen that the method based on time difference introduced less errors than the one based on relative frequency error. However, the calculation

model of Allan variance presented in this paper can only reflect the overall distribution of two USOs' relative frequency stability to a certain extent, but not the exact frequency stability of a single USO. While, what needs to be known is that for the data post-processing of KBR data, monitoring the distribution and change trend of USO frequency stability in a certain period of time has already played a very significant role in the effectiveness interpretation of payloads data. The research results of this paper have some reference to the design of inter-satellite ranging system of Chinese first generation earth gravity exploration satellite.

References

1. Wang Z, Jiang W (2011) Theory and method of determining the earth's gravitational field based on satellite tracking satellite technology. Wuhan University Press, Wuhan, pp 5–13
2. She S, Wang K (2006) The technology of high accuracy inter-satellite microwave ranging. J Astronaut 3:402–406
3. Kang K, Li H (2012) Demonstration on the design of filter indexes of inter-satellite high accuracy ranging system for gravity satellite. Chin J Geophys 10:55–110
4. Liu X, Wang D et al (2015) Research on the effect of signal propagation delay between satellites on KBR's measurement performance. In: Academic conference proceedings of China aerospace institute in 2015
5. Kim J, Tapley BD (2003) Simulation of dual one-way ranging measurements. J Spacecraft Rockets 40(3):419–425
6. Thomas JB (1999) An analysis of gravity-field estimation based on inter-satellite dual-1-way biased ranging, Jet Propulsion Lab. JPL Publications. 98-15, Pasadena, CA, May 1999
7. Zhong C, Xia Z (2008) Transform of short-term frequency stability from frequency domain to time domain. The frequency control technology conference proceedings in 2008

Research of Satellite and Ground Time Synchronization Based on a New Navigation System

Yang Yang, Yufei Yang, Kun Zheng and Yongjun Jia

Abstract The new navigation time synchronization method is a breakthrough in existing navigation systems time synchronization accuracy limit, and it is an effective way to reduce system construction costs. By placing more accurate atomic clock in GEO satellites, it can synchronize with ground systems and generate time reference, the GEO satellites can give time to other navigation satellites, the new system can achieve high-precision time synchronization. This paper designs the navigation constellation of the new satellite navigation system, and configures the satellite clocks, simulates all kinds of constellation time synchronization precision, and educes the satellite clock configure scheme in the new navigation system.

Keywords Navigation system · Time synchronization · Satellite clock

1 Introduction

Satellite navigation systems have been widely used in military and civilian aspects of various countries and have achieved great benefits. But still there are various disadvantages in navigation system, as the number of existing satellite onboard atomic clocks demands more and high costs [1, 2]. Therefore, the use of new atomic clock design, to explore new satellite clock configuration is an effective way to reduce system construction costs.

The new time synchronization method is essentially a kind of satellite-ground, inter-satellite system operation control concept: it contains GEO satellites constellation and high accurate atomic clock; its time reference is generated by the GEO satellites and the system Control Segment Operational; it mainly relies on the OCS to do the centralized satellite-ground and inter-satellite measurement

Y. Yang (✉) · Y. Yang
Beijing Satellite Navigation Centre, Beijing, China
e-mail: 112632507@qq.com

K. Zheng · Y. Jia
Beijing Institute of Special Electromechanical Technology, Beijing, China

J. Sun et al. (eds.), *China Satellite Navigation Conference (CSNC) 2016 Proceedings: Volume III*, Lecture Notes in Electrical Engineering 390,
DOI 10.1007/978-981-10-0940-2_2

processing; it depends on the inter-satellite link to update the ephemeris, and to shorten the data age. So, non-GEO satellite of the navigation constellation can use reasonable algorithm, high-precision satellite-ground and inter-satellite link, and the configuration of the ultra-stable crystal oscillator, to achieve a high precision with low construction cost.

2 The New Time Synchronization Plan

Under the new system time synchronization plan involved basic navigation constellations and star clock design, the link design, and time synchronization plan.

This system needs GEO satellite to provide time service, so the constellation must contain GEO satellites. For new time synchronization system, GEO satellites use more accurate onboard atomic clock which builds a time reference together with the OCS clock [3]. This paper takes two types of optical clocks and hydrogen atomic clock as a time reference installed on the GEO satellite, and non-GEO satellites use ordinary onboard atomic clock or ultra-stable crystal oscillator. The new time synchronization system involves satellite-ground link and inter-satellite link. Inter-satellite link contains timing link between GEO and non-GEO satellite and time synchronization link between non-GEO satellites. The new time synchronization method contains that: non-GEO satellites-ground link use satellite time and frequency transfer method; inter-satellite link use inter-satellite two-way time and frequency transfer method; GEO satellite-ground link use both satellite laser ranging and two-way time and frequency transfer method; OCS and each time synchronization stations use both satellite two-way time and frequency method and satellite common-view method.

3 Time Synchronization Measurement Model

The satellite-ground microwave observation model can be expressed as [4]:

$$\rho' = \rho + c \cdot (\Delta t_S - \Delta t_R) + \Delta\rho_{\text{ion}} + \Delta\rho_{\text{tro}} + \Delta\rho_{\text{rel}} + \Delta\rho_{\text{scc}} + \Delta\rho_{\text{ant}} + \Delta\rho_{\text{ml}} + \varepsilon \quad (1)$$

In this formula, ρ' is microwave observation value, ρ is the true distance from the ground station to the satellite; c is the light speed, Δt_S is satellite clock error, and Δt_R is ground station clock error; $\Delta\rho_{\text{ion}}$ is ionospheric delay error, $\Delta\rho_{\text{tro}}$ is tropospheric delay error; $\Delta\rho_{\text{rel}}$ is relative delay error; $\Delta\rho_{\text{scc}}$ is satellite centroid compensation correction; $\Delta\rho_{\text{ant}}$ is antenna phase center error; $\Delta\rho_{\text{ml}}$ is multipath effect; ε is pseudo range observation noise.

The satellite-ground laser observation model

The observation model of the satellite-ground laser ranging can be expressed as:

$$\rho' = \rho + \Delta\rho_{\text{tro}} + \Delta\rho_{\text{rel}} + \Delta\rho_{\text{scc}} + \Delta\rho_{\text{ec}} + \Delta\rho_{\text{ant}} + \Delta\rho_{\text{ml}} + \varepsilon \tag{2}$$

In this formula, ρ' is laser observation value. ρ is the true distance from the laser station to the satellite; $\Delta\rho_{\text{tro}}$ is tropospheric delay error; $\Delta\rho_{\text{rel}}$ is relative delay error; $\Delta\rho_{\text{scc}}$ satellite centroid compensation correction; $\Delta\rho_{\text{ec}}$ is station coordinate correction; $\Delta\rho_{\text{ant}}$ is antenna phase center error; $\Delta\rho_{\text{ml}}$ is multipath effect; ε is laser observation noise.

Two-way measurement equation

The two-way measurement equation can be obtained from the single direction measurement equation of satellite-ground and inter-satellite.

$$\begin{cases} \bar{\rho}_{ij} = d + c \cdot \delta t_i - c \cdot \delta t_j + n_{ij} \\ \bar{\rho}_{ji} = d + c \cdot \delta t_j - c \cdot \delta t_i + n_{ji} \end{cases} \tag{3}$$

In this formula, $\bar{\rho}_{ij}$ and n_{ij} are pseudorange (microwave, laser) and measurement noise from point S_i to S_j; $\bar{\rho}_{ji}$ and n_{ji} are corrected pseudorange (microwave, laser) and measurement noise from satellite S_i to S_j; δt_i and δt_j are clock error S_i and S_j. c is the light speed and d stands for distance between S_i and S_j, as below: $d = [(x_i - x_j)^2 + (y_i - y_j)^2 + (z_i - z_j)^2]^{1/2}$.

4 Satellite Clock Modeling and Time Synchronization Algorithm

The atomic clock used in the satellite navigation system contains system change and random error. Atomic clock error may be expressed as the difference between the instantaneous clock time and the standard time $x(t)$. Choose quadratic polynomial model as clock error model

$$x(t) = a_0 + a_1(t - t_0) + \frac{1}{2}a_2(t - t_0)^2 + \varepsilon_x(t) \tag{4}$$

In this formula, a_0 is the initial phase(time) deviation, a_1 is the initial deviation of the atomic clock frequency, and a_2 is linear frequency drift rate; $\varepsilon_x(t)$ is the random variation component of clock deviation caused by clock noise; t_0 is the reference time. The step of time synchronization process is as follows: observation data pretreatment, parameters priori information determination, initial clock error calculation, time estimation matrix building, residual edit, and iteration [5].

5 Simulation and Results Analysis

5.1 Atomic Clock and Clock Data Simulation

Allan variance is the most common expression of frequency stability, which depends on the length of time stability, and is divided into short-term frequency and long-term stability. Although the definition of short-term stability and long-term frequency stability is same, they reflect different aspects of signal stability characteristics. Measurement of short-term frequency stability in the time domain is very difficult, or even impossible, but at the same time it is easier to measure in the frequency domain. So, short-term frequency stability measurement can be converted into a time domain phase noise, so as to get the short-term time domain stability indirectly. Phase noise theory and statistical thin phase noise of time domain and frequency domain Allan variance are equivalent. If got the conversion relationship between them, the amount of each physical characterization can be then revealed. This paper use Allan variance as the satellite clock error calculation model.

When calculating the simulation, noise as above is generated by the white noise, and relevant noise generation process is as follows [6]:

$$y_i^{\mathrm{WP}} = \sigma_{y\mathrm{WP}}(\tau) \cdot (\mathrm{rand}_i - \mathrm{rand}_{i-1}) y_i^{\mathrm{WF}} = \sigma_{y\mathrm{WF}}(\tau) \cdot \sqrt{3} \cdot \mathrm{rand}_i$$
$$y_i^{\mathrm{RW}} = y_{i-1}^{\mathrm{RW}} + \sigma_{y\mathrm{RW}}(\tau) \cdot 3 \cdot \mathrm{rand}_i$$
$$y_i^{\mathrm{FF}} = \sigma_{y\mathrm{FF}}(\tau) \cdot \sqrt{5} \cdot [i^{-2/3}\mathrm{rand}_1 + (i-1)^{-2/3}\mathrm{rand}_2 + (i-2)^{-2/3}\mathrm{rand}_3 + \cdots + \mathrm{rand}_i]$$

In this formula, $\mathrm{rand}_i \sim N(0,1)$, N is the number of sampling points.

Atomic clock error is calculated by the following formula:

$$x_i = x_{i-1} + \tau(y_i^{\mathrm{WP}} + y_i^{\mathrm{WF}} + y_i^{\mathrm{FF}} + y_i^{\mathrm{RW}}) \quad i = 1, 2, \ldots N \tag{5}$$

5.2 Simulation of Ultra-Stable Oscillator Data

Crystal error is more complex, so there is no proper mathematical model yet. Since there is no direct ultra-stable oscillator laboratory results, this paper uses Allan variance provided by ACES. Inverse the main Allan variance noise component, and put them together (Table 1).

Table 1 ACES ultra-stable crystal oscillator (USO) Allan variance with interval

Measurement interval (s)	1	2	4	10	20
Sigma	1.49e−13	1.26e−13	1.00e−13	8.82e−14	8.88e−14
Interval (s)	40	100	200	400	1000
Sigma	9.67e−14	1.23e−13	1.30e−13	1.20e−13	2.25 e−13

Table 2 Calculated Allan variance of noise figure

h_{-2}	h_{-1}	h_0	h_1	h_2
1.00e−13	8.82e−14	8.88e−14	9.67e−14	1.23e−13

With the condition of knowing Allan variance value of five typical time interval τ, h_{-2}, h_{-1}, h_0, h_1, h_2 can be calculated; knowing more than five Allan variance value, it can be calculated by least squares method, and then calculate any corresponding Allan variance (Table 2).

Because the random walk, frequency flicker noise, frequency white noise, flicker phase noise, and phase noise are independent random processes, after separated apart, five noises can use its own characteristic to inverse error sequences.

You can utilize these five separate noises respective characteristics, separated these noises and inversion error sequence, the formula shows in Eq. (5).

5.3 Simulation Conditions

In this paper, navigation constellation consists of MEO, GEO, and IGSO numbered 1–35, of which No. 1–27 is MEO satellites, No. 28–30 is IGSO satellite, and No. 31–35 is GEO satellite. Inter-satellite link error is set to 0.1 m (1σ). Satellite-ground link error is analyzed in two ways: Microwave satellite-ground microwave link error is 1.2 m (1σ); Laser microwave link error is 0.1 m (1σ).

There are five domestic time synchronization stations, whose minimum elevation observations are 5°. The simulation period is 7 days. Onboard satellite clock error, initial onboard clock error σ_{X_0}, and covariance matrix P_{X_0} of hydrogen maser, rubidium and cesium clock, optical clocks, ultra-stable oscillator is as [7, 8].

The simulation program is in Table 3.

Table 3 Simulation algorithm design

Scenario	Station	GEO	Non-GEO	Measurement
I	Hydrogen	Cesium	Rubidium/Cesium	Microwave satellite-ground link + Ka inter-satellite links
II	Optical	Optical	Rubidium + Cesium	Microwave satellite-ground link + Ka inter-satellite links
III	Optical	Optical	Ultra-stable oscillator	Microwave and laser joint satellite-ground link + Ka inter-satellite link
IV	Optical	Hydrogen	Rubidium + Cesium	Microwave and laser joint satellite-ground link + Ka inter-satellite link
V	Optical	Hydrogen	Ultra-stable oscillator	Microwave and laser joint satellite-ground link + Ka inter-satellite link

5.4 Simulation Results Analysis

Figures 1 and 2 are traditional satellite time synchronization error statistics. Without navigation constellation two-way filtering time synchronization, or entire constellation drift time, which maximum drift is about 7 ns, the introduction of inter-satellite links increased redundancy observations to help improve the time synchronization accuracy, to keep constellation drift within 0.65 ns in simulation conditions.

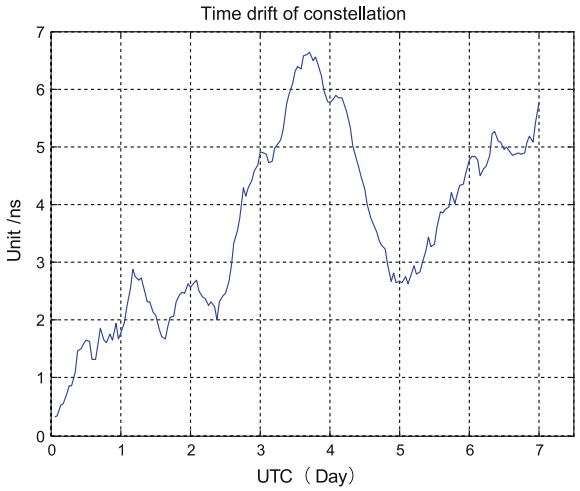

Fig. 1 Option I: constellation time drift error

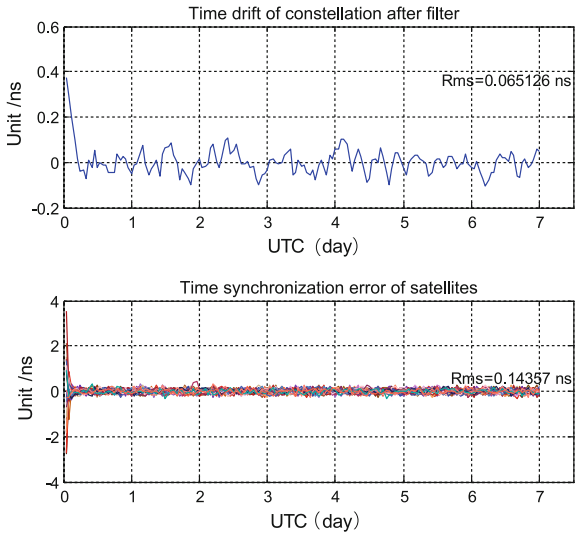

Fig. 2 Option I: constellation drift and satellite time synchronization error

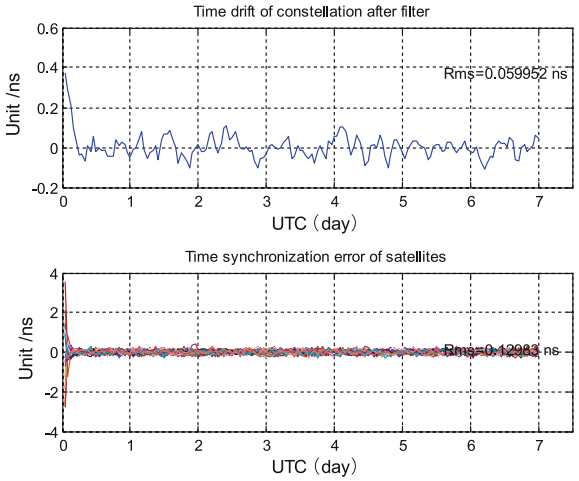

Fig. 3 Option II: constellation drift and satellite time synchronization error

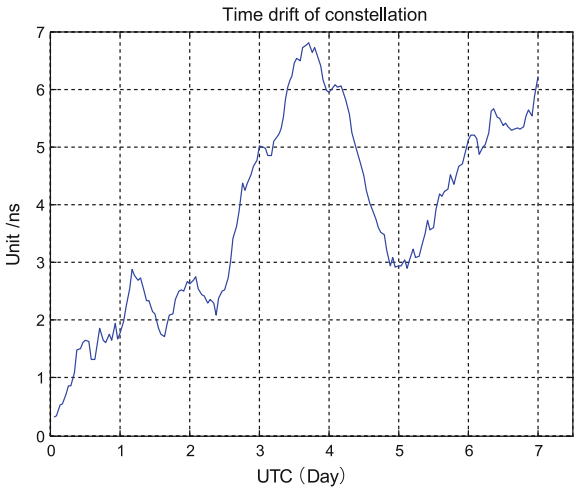

Fig. 4 Option II: constellation time drift error

Figures 3 and 4 are atomic clock + atomic clock(rubidium, cesium). Due to the GEO satellite uses a high-precision optical clocks, the simulation use laser and microwave joint satellite-ground link to take place traditional satellite-ground link; the clock of ground station is optical clock; GEO equipped with optical atomic clock; GEO onboard clock does not participate in time synchronization between non-GEO satellites, and only do time synchronization with ground stations to keep time reference. The time reference in this paper is time reference in navigation system with respect to UTC, not taking the establishment of optical clocks to improve the accuracy of UTC time in consideration. Figure 3 shows that the average constellation time (the constellation drift) and constellations time synchronization accuracy with respect to the traditional model has greatly improved.

At a given simulation conditions, the constellation average time is below 0.06 ns, time synchronization accuracy is below 0.14 ns, non-filtering time synchronization under the same conditions as a whole constellation of synchronization drift reached 7 ns (Fig. 4).

Figures 5 and 6 are the time synchronization accuracy of new optical atomic clock + ultra-stable oscillator clock. Ultra-stable oscillator has a good short-term stability but a poor long stability. Without two-way time synchronization, the whole constellation time shift is about 140 ns (Fig. 6), much larger than the drift of rubidium and cesium clock (Fig. 4). However, when added microwave and laser joint satellite-ground link, the average constellation time (the constellation drift) accuracy is about 0.0488 ns (Fig. 5). Which is slightly better than optical II.

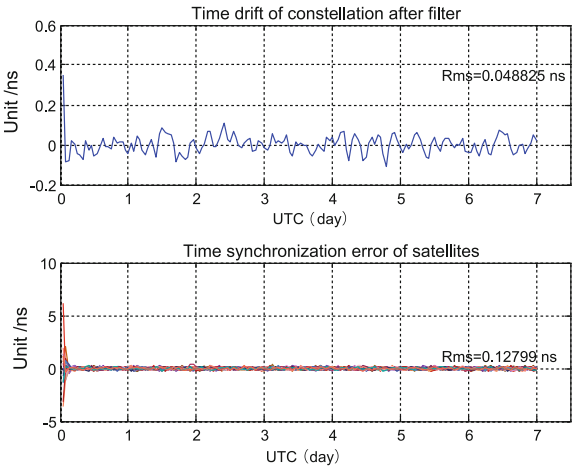

Fig. 5 Option III: constellation drift and satellite time synchronization error

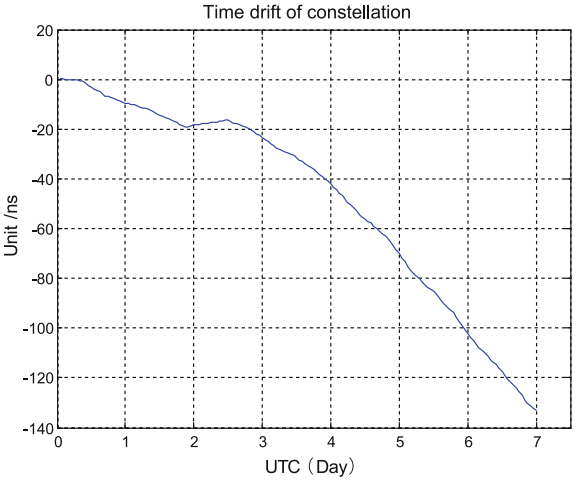

Fig. 6 Option III: constellation time drift error

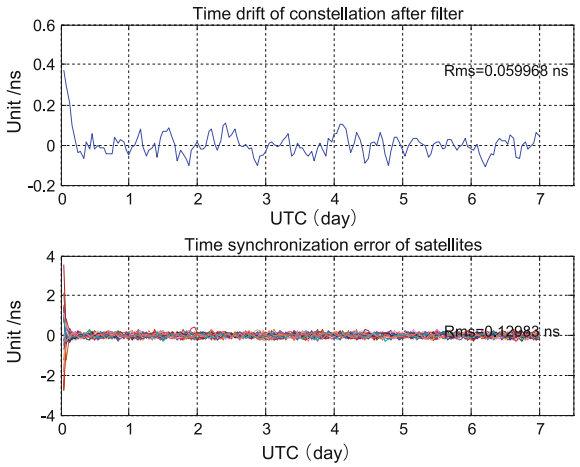

Fig. 7 Option IV: constellation drift and satellite time synchronization error

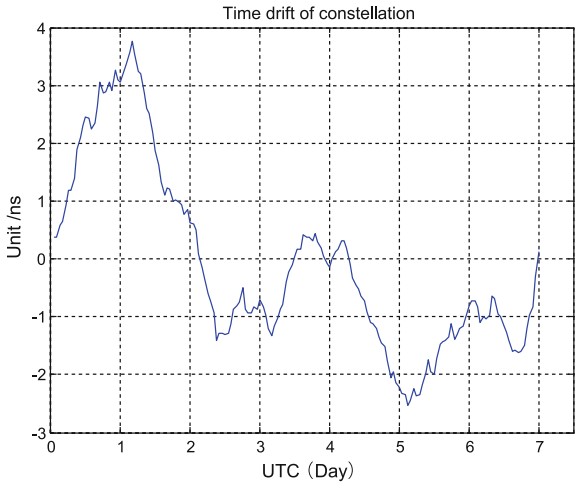

Fig. 8 Option IV: constellation time drift error

Figures 7 and 8 are the time synchronization accuracy of new hydrogen atomic clock + atomic clock(rubidium, cesium). As can be seen from Fig. 7, the average constellation two-way filtering time accuracy is 0.06 ns, time synchronization accuracy is 0.13 ns, and the average two-way filtering time is considerable with option II and III. The time synchronization accuracy of each satellite is lower than option II and III (Fig. 8).

Figures 9 and 10 are the time synchronization accuracy of new hydrogen atomic clock + ultra-stable oscillator clock. GEO is equipped with hydrogen atomic clock; other satellite clock uses ultra-stable oscillator clock. It can be concluded that the overall constellation time drift is about 0.05 ns, time synchronization accuracy is 0.128 ns (Fig. 9). Under the given simulation condition, the accuracy is slightly

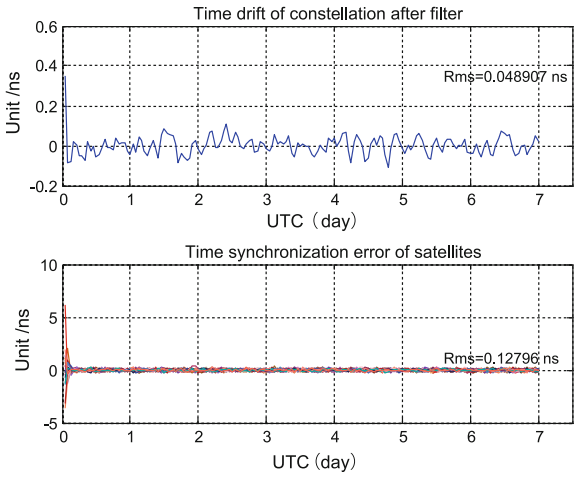

Fig. 9 Option V: constellation drift and satellite time synchronization error

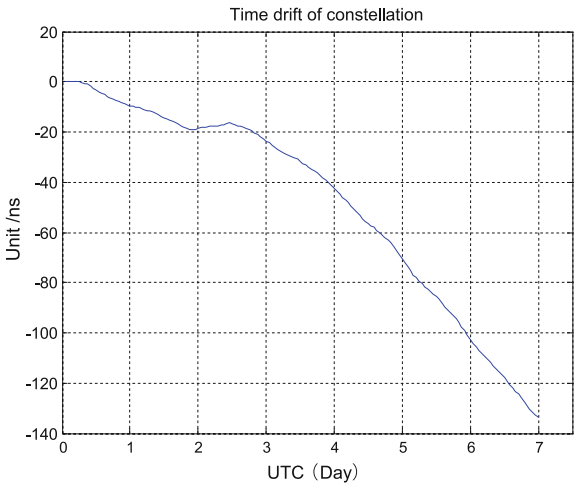

Fig. 10 Option V: constellation time drift error

better than option IV (Fig. 10). The time synchronization accuracy is slightly better than the option IV too.

5.5 In Conclusion

The present problem of onboard atomic clock frequency drift, accuracy will be getting worse with time. In this paper, simulation results show that:

The new time synchronization method can greatly improve the time synchronization accuracy.

In the new satellite and ground joint batch processing mode, the accuracy of hydrogen atomic clock and atomic clock on the GEO satellite is at the same orders of magnitude. This is because: when the satellite and ground joint estimation, all observations is transform to the same epoch, and the overall network adjustment make full use of observation information, in order to improve time synchronization accuracy. When the satellite and ground joint estimation, time synchronization accuracy depends on the satellite, the inter-satellite link precision, and algorithms. When GEO is equipped with optical atomic clock, its stability is about 1.25×10^{-12} s, the stability of hydrogenatomic clock is about 6.25×10^{-11}. In the simulation, the satellite-ground link accuracy is about 0.1 m, and the time synchronization error is about 3×10^{-10} s, the noise of satellite-ground link drowned GEO onboard clock performance, so with respect of satellite and ground joint entire network time synchronization, the accuracy of optical atomic clock and hydrogen atomic clock on the GEO satellite is at the same orders of magnitude.

Under the condition of new method, the ultra-stable oscillator can replace rubidium, cesium clock as onboard atomic clock of non-GEO satellites.

References

1. Gill P, Margolis H, Curtis A et al (2008) Optical atomic clocks for space. National Physical Laboratory
2. Godone A, Levi F, Micalizio S et al (2004) Coherent population trapping maser: noise spectrum and frequency stability. Phys Rev A 70(1):2508–2519
3. Svehla D (2008) A novel design for the navigation system and proposal to unify the timing and the positioning system using GIOVE Follow-on. ACES and future GNSS-based earth observation and navigation, Munich, Germany, 26–27 May 2008, pp 1–27
4. Kou Y (2007) GPS principles and applications. Publishing House of Electronics Industry, Beijing
5. Zhu J. The study of navigation satellite orbit determining and time synchronization method for ISLs. National University of Defense Technology(Ch), Changsha
6. Svehla D, Rothacher M, Ziebart M, Salomon C (2006) Galileo on board International Space Station and synergy with the ACES clock ensemble. European Geophysical Union, General Assembly, Vienna, 2–7 April 2006, pp 1202–1210
7. Diez J, D'Angelo P, Fernández A (2006) Clock errors simulation and characterisation. ION GNSS 19th international technical meeting of the satellite division, Fort Worth, Texas, 2006, pp 815–821
8. Weaver G (2010) The performance of ultra-stable oscillators for the gravity recovery and interior laboratory. 42nd annual precise time and time interval (PTTI) meeting, 2010, pp 369–379

Performance Evaluation of the Beidou Satellite Clock and Prediction Analysis of Satellite Clock Bias

Xueqing Xu, Shanshi Zhou, Si Shi, Xiaogong Hu and Yonghong Zhou

Abstract Satellite clock bias (SCB) is provided by the in orbit atomic clock, which is the key to satellite navigation system. First, the time reference of the satellite navigation system is realized by the SCB, and the SCB prediction accuracy will also affect the positioning accuracy of real-time navigation users. With the development of our Beidou satellite navigation system (BDS), the performance requirement of the satellite clock and accuracy requirement of the SCB prediction are higher and higher. This paper will study on performance evaluation of BDS atomic clock and the prediction analysis of SCB series exclusively. In order to show the results objectively and effectively, we select two data processing centers of the GeoForschungsZentrum Potsdam (GBM), and SHAO Analysis Center (SHA), to obtain the same time BDS clock bias sequence as the base data, for a comparative analysis. First, the performance of the atomic clock is evaluated by statistics of the Allen variance. Meanwhile, we establish the model for each SCB sequence according to the characteristic of the atomic clock, by using a combined method of least squares and autoregressive model (LS+AR), to predict and assess the SCB with root mean square error (RMS). Results show that the performance of BDS in orbit atomic clock is stable, with the day stability in the order of 10^{-14}; And the atomic clock performance is related to the SCB prediction accuracy, that is shown as better performance with higher prediction accuracy; Mean while the LS+AR model predict SCB series based on the performance of different atomic clocks, which can improve the SCB prediction accuracy effectively.

X. Xu (✉) · S. Zhou · S. Shi · X. Hu · Y. Zhou
Shanghai Astronomical Observatory, Chinese Academy of Sciences,
Nandan Road no. 80, Xuhui District 200030, Shanghai, China
e-mail: xqxu@shao.ac.cn

X. Xu · X. Hu · Y. Zhou
Key Laboratory of Planetary Sciences, Chinese Academy of Sciences,
Shanghai 200030, China

S. Shi
Graduate University of Chinese Academy of Sciences, Beijing 100049, China

J. Sun et al. (eds.), *China Satellite Navigation Conference (CSNC) 2016 Proceedings: Volume III*, Lecture Notes in Electrical Engineering 390,
DOI 10.1007/978-981-10-0940-2_3

Keywords Atomic clock performance · Allen variance · SCB prediction · Least squares · Autoregressive model

1 Introduction

BeiDou Navigation Satellite System (BDS) is a global satellite positioning and communication system developed by China, which contains three departments of the space part, the ground part, and the customer part, and can provide the users with high precision and reliable positioning, navigation and timing services globally and all-weather, and has a short message communication ability. Now the BDS can provide regional navigation, positioning, and timing services. The space constellation of BDS consists of 14 satellites, and each satellite is equipped with four high performance rubidium atomic clocks, one of them is as a measurement of time, and the rest are standby as the spare. The error sources which influence the accuracy of satellite orbit determination are mainly derived from the orbit and satellite clock. The performance of atomic clock has a direct impact on the accuracy of satellite clock bias (SCB) observations and predictions, which will affect the accuracy of satellite orbit determination [4, 12]. The performance of in orbit atomic clock maybe changed with the variation of space environment, in order to effectively control the characteristic of atomic clock (stability), it is important to evaluate the performance of the in orbit satellite clock.

The SCB reliable prediction is also important for satellite navigation, especially for orbit determination of the autonomous navigation satellite. During the space running period, if satellite gets into the arcs that cannot be observed by ground stations, then the atomic clock cannot be compared to the ground time reference. The synchronization between satellite clock and the system time should be maintained by satellite clock itself, which is the prediction of SCB. While the prediction accuracy of SCB is affected by the physical characteristics of atomic clock, which is the performance of in orbit satellite clock mentioned above, but also related with the prediction method [7, 9]. Now the mostly used forecasting models about the SCB are: (1) the linear model (LM) [3, 13], (2) the quadratic polynomial model (QPM) [5, 6]. These prediction methods are simple and suitable for prediction of the regular terms in SCB series, which is the part that can be expressed by quadratic polynomial or periodic function, while ignoring the prediction of the irregular part that cannot be directly expressed by the fitting model, and the SCB prediction accuracy will be restricted.

Considering the points above, this paper selects the two data processing centers of GeoForschungsZentrum Potsdam (GBM), and the Shanghai Observatory Data Analysis Center (SHA), and gets the same time BDS clock sequence as the base data. First, the performance of the atomic clock is evaluated by statistics of the Allen variance. On the other hand, we investigate a combined method of least squares and auto regression model (abbreviated as LS+AR), to establish the model for each SCB sequence according to the characteristic of the atomic clock,

and predict the SCB sequences with prediction accuracy assessment by root mean square error (RMS), which draw lessons from our mature experience in the Earth Orientation Parameters (EOP) forecasting [10, 11].

2 Models

In this work, we first analyze the different SCB data series of two processing centers, with the Allen variance to evaluate the frequency stability of the Beidou satellite atomic clock. Construct a fitting model that mainly contains quadratic term and periodic terms, to separate the regular and irregular terms in SCB sequence, then the fitting model is used for prediction of SCB regular terms, and an AR (p) model is selected as the prediction model for SCB irregular terms. The principles of Allen variance for performance evaluation, fitting models, and AR (p) model are briefly described as follows.

2.1 Performance Evaluation

The stability of atomic clock frequency is a key factor of the real-time positioning performance, and Allen variance is generally used to evaluate the frequency stability. Allen variance, which is also known as the double sampling variance, and at first was used to analyze the phase and frequency instability of the oscillator, and then was defined as the common frequency stability analysis method by IEEE standard [8]. Here we select the Allen variance to evaluate the frequency stability of atomic clock, the standard Allen variance is defined as:

$$\sigma_y^2(\tau) = \frac{1}{2(M'-1)} \sum_{k=1}^{M'-1} (\bar{y}_{k+1} - \bar{y}_k)^2, \tag{1}$$

where

$$\bar{y}_k = \frac{x(t_k + \tau) - x(t_k)}{\tau}. \tag{2}$$

where $x(t_k)(t_k = 1, 2, \ldots, N)$ is SCB series, $\bar{y}_k(k = 1, 2, \ldots, N)$ is the average fractional frequency over a specified interval of interest τ, τ is the sample interval.

2.2 Prediction Model for Regular Terms

Because of the different characteristic of the atomic clock, we construct different fitting models to separate the regular and irregular parts in SCB sequence. For the fitting model, we first identify the main periods of SCB sequence by the spectral analysis method, and then establish the model mainly contains the constant term, linear term, quadratic term, and periodic terms, where the main periods in the SCB sequence are 1 week, 24, 12, and 6 h [8]. The fitting model is expressed as,

$$Y_t = a_0 + a_1 t + a_2 t^2 + \sum_{k=1}^{4} b_k \sin(2\pi t/P_k + \phi_k) + \varepsilon_t \tag{3}$$

where, a_0 is the constant term, a_1 is the linear coefficient, a_2 is the quadratic coefficient, t is time, P_k, b_k and ϕ_k are period signals, amplitude, and phase of periodic signals in satellite clock errors sequence, and ε_t is the noise.

After the regular and irregular parts in SCB sequence are isolated by fitting the clock error sequences, the fitting model is then used as the prediction model of the SCB irregular terms. According to the principle of least squares, the predictions of the SCB regular terms can be extrapolated by the fitted model coefficients above.

2.3 Prediction Model for Irregular Terms

The SCB regular terms can be extrapolated by the fitting model smoothly, while the irregular parts in the SCB series are difficult to predict by a simple fitting model, which should be derived by other methods, here we select the classical autoregressive model (AR model). For a stationary random sequence $z_t (t = 1, 2, \ldots, N)$, the p order of AR model (AR(p)) is expressed as follows,

$$z_t = \sum_{i=1}^{p} \varphi_i z_{t-i} + a_t. \tag{4}$$

where, a is zero-mean white noise, p is order of the model, $\varphi_1, \varphi_2, \ldots, \varphi_p$ are autoregressive coefficients.

We adopt the final prediction error criterion (FPE) to identify the order p of AR model for each forecasting step, which corresponds to the smallest FPE [1]. The coefficients can be obtained for solving the Yule-Walker equations by means of the Burg recursion [2] method. Based on the above methods, the AR (p) model can

be updated for each forecasting step, and the new AR (p) model is more reasonable and accurate.

$$\mathrm{FPE}(p) = \mathrm{P}_p(N+p+1)/(N-p-1), \tag{5}$$

$$\mathrm{P}_p = 1/(N-p)\sum_{t=p+1}^{N}\left(z_t - \sum_{j=1}^{p}\varphi_j z_{t-j}\right)^2. \tag{6}$$

where, N is the number of the data sequence $z_t(t = 1, 2, \ldots, N)$, P_p is the rest mean square error.

3 Calculation Example

At present, there are 14 working satellites in the BDS network, forming a regional navigation and positioning system. This network includes five geostationary satellites (GEO, C01–C05), four middle orbit altitude satellites (MEO, C06–C09), and five periodic tilted earth synchronous orbit satellites (IGSO, C10–C14). Among them, the C13 satellite does not work temporarily, which is unable to obtain the SCB data, and is not included in this article.

This work employs the SCB sequence from the two data analysis center GBM and SHA. First the Allen variance was carried out, to comparatively analyze the frequency stability of BDS atomic clock in different time scales; and then used a combined LS+AR method for SCB short term forecasting, the prediction accuracy verification is obtained by comparing the model predicted values with clock bias data, where the prediction spans are mainly selected as 2, 6, and 12 h.

3.1 Prediction Error Estimates

For the estimation of SCB prediction accuracy, we select the root mean squared error (RMS) as the indicator.

$$\mathrm{RMS}_i = \sqrt{\frac{1}{n}\sum_{j=1}^{n}\left(p_j^i - o_j^i\right)^2} \tag{7}$$

where, o is the SCB observations, p is the SCB predictions, i is the prediction interval, n is the number of total predictions.

3.2 Result Analysis

Allen variance of the SCB sequences is first calculated to evaluate stability of the BDS atomic clocks on different scales, and the results were counted in Table 1. In order to intuitively show the stability of the BDS satellite clock presented by two different processing centers, the representative C01 satellite with continuous and complete SCB data is selected as an example, whose Allan variance results on different time scales are plotted in Fig. 1.

For the SCB sequences of two processing centers, 200 predictions are made by means of LS+AR method, with prediction interval of 2, 6, and 12 h, and the mean square error (RMS) is calculated and listed in Table 2, the unit is nanoseconds (ns). In order to show the trend of the forecast error with time increasing, the C01 satellite is also selected as an example, whose 12 h SCB prediction errors in future of the two processing centers are plotted in Fig. 2.

Table 1 Statistics about the Satellite clock stability of processing center GBM and SHA

Sat/Allen variance	GBM		SHA	
	100,000 s	1,000,000 s	100,000 s	100,0000 s
C01	1.354e−13	1.317e−14	6.865e−14	1.323e−14
C02	2.863e−13	4.546e−14	2.124e−13	3.098e−14
C03	1.175e−13	3.352e−14	1.105e−13	2.125e−14
C04	1.052e−13	2.708e−14	7.388e−14	2.913e−14
C05	1.104e−13	3.248e−14	8.102e−14	1.743e−14
C06	1.981e−13	4.314e−14	2.321e−13	3.805e−14
C07	9.015e−14	2.682e−14	7.955e−14	2.213e−14
C08	1.969e−13	3.921e−14	2.098e−13	4.336e−14
C09	1.207e−13	3.457e−14	9.478e−14	3.304e−14
C10	1.940e−13	4.603e−14	2.013e−13	4.046e−14
C11	1.545e−13	3.143e−14	1.285e−13	3.502e−14
C12	1.031e−13	3.047e−14	8.145e−14	3.206e−14
C14	9.389e−14	2.985e−14	9.069e−14	3.085e−14

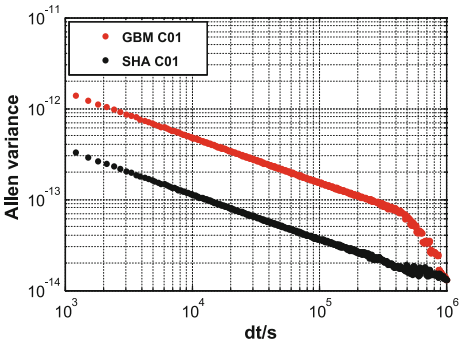

Fig. 1 Satellite clock stability comparison of different time scales of GBM and SHA C01

Table 2 Statistics about the Satellite clock prediction error of processing center GBM and SHA

Sat/RMS	GBM			SHA		
	2 h/ns	6 h/ns	12 h/ns	2 h/ns	6 h/ns	12 h/ns
C01	0.447	1.194	2.582	0.383	0.976	2.109
C02	1.315	3.975	8.977	1.454	4.724	9.287
C03	0.473	2.003	4.407	0.538	2.334	4.696
C04	0.872	2.740	5.897	0.651	2.603	5.198
C05	0.509	1.813	3.415	0.524	1.798	3.271
C06	0.809	3.041	6.524	1.108	3.201	6.754
C07	0.516	1.605	3.245	0.665	1.974	4.031
C08	1.024	3.254	7.479	1.113	4.025	8.492
C09	0.912	1.831	3.858	0.592	1.404	3.517
C10	0.893	3.126	7.273	1.152	3.478	7.972
C11	0.539	1.569	5.102	0.471	1.762	5.119
C12	0.563	1.724	5.756	0.547	1.895	5.937
C14	0.889	3.062	5.698	0.745	2.759	5.477

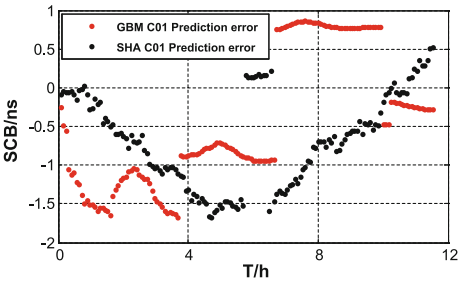

Fig. 2 Satellite clock 12 h prediction error comparison of GBM and SHA C01

Some conclusions can be obtained from the above charts and figures:

(1) we can get some information from Table 1 and Fig. 1, with comparative analysis about the SCB Allan variance of two data processing center, that the current BDS in orbit satellite atomic clock frequency stability is consistent, which is 10^{-13} to 10^{-14} at one hundred thousand second, and 10^{-14} at 1 day.

(2) the SCB predictions of two data processing centers are calculated by using the combined least squares and regression model (LS+AR), the prediction error estimation results in Table 2 and Fig. 2, show that the prediction accuracy performance of satellite C02, C08, C06, and C10 is inferior slightly, mainly due to the quality of the satellite clock itself, while the others present a high prediction accuracy, with 2 h of lower than 1 ns, 6 h of about 2 ns, and 12 h of about 5 ns.

(3) combined the results in Table 1 with Table 2, we find that the satellite (C02, C06, C08, and C10) with poor performance of SCB prediction accuracy,

whose frequency stability of atomic clock is relatively poor, which shows that the stability of the satellite atomic clock will affect the prediction accuracy of the SCB, it further shows that the LS+AR method is effective and necessary by modeling and forecasting the SCB series for each satellite.

4 Conclusion

In this study, the BDS SCB data were obtained from two data processing centers of GBM and SHA. The Allen variance is first listed for comparison analysis on the frequency stability of different satellite atomic clocks. Then we perform the modeling of the SCB sequence for each satellite, by means of LS+AR method, to separate the SCB regular and irregular terms, and their predictions is carried out respectively. Then the prediction accuracy is obtained by comparing the model predicted values with original data.

Here are some conclusions: first, the frequency stability of the BDS in orbit satellite atomic clock shows consistent performance, with 10^{-13} to 10^{-14} at one hundred thousand second, and 10^{-14} at 1 day. Second, the mostly BDS SCB series present a high prediction accuracy, with 2 h of lower than 1 ns, 6 h of about 2 ns, and 12 h of about 5 ns. At the same time, the stability of the satellite atomic clock will affect the prediction accuracy of the SCB, which is shown as better stability performance with higher prediction accuracy relatively. This study uses the LS+AR model to establish the model of the SCB sequence for each satellite, and forecast the SCB regular and irregular terms, respectively, which avoids the problem that error accumulation increases sharply with the increase of the forecast span, in the simple quadratic prediction model,and improve the SCB prediction accuracy remarkably.

Acknowledgments The research is supported by the NSFC grant (11303073, 41574029, 11373057, 11133004), STCSM (06DZ22101). We thank GeoForschungsZentrum Potsdam (GBM) and SHAO Analysis Center (SHA) for providing the GPS SCB data.

References

1. Akaike H (1971) Autoregressive model fitting for control. Ann Inst Stat Math 23:163–180
2. Brockwell PJ, Davis RA (1996) Introduction to time series and forecasting. Springer, New York
3. Dai W, Jiao W, Li W (2009) Research on prediction of GPS B lock IIR (M) atomic clock error. J Geodesy Geodyn 29(4):111–115
4. Gao W, Lin Y, Chen G, Meng Y (2014) The performances assessment methods and results of in-orbit atomic clocks of BDS. J Geomatics Sci Technol 31(4):342–346
5. Guo H, Yang S, Yang Y (2007) Numerical prediction methods for clock difference based on two-way satellite time and frequency transfer data. Geomatics Inf Sci Wuhan Univ 32(1):43–46

6. Liu X, Wu X, Tian Y (2010) Study on atomic prediction of time based on interpolation model with tchebytchev polynomials. J Geodesy Geodyn 30(1):77–82
7. Liu Y, Dang Y, Zheng Z (2011) Study and improvement for the model in satellite clock error long-term forecast. Hydrographical Surveying Charting 31(2):21–23
8. Senior KL, Ray JR, Beard RL (2008) Characterization of periodic variations in the GPS satellite clocks. GPS Solution 12:211–225
9. Tang G, Xu X, Cao J, Liu X, Wang Q (2015) Precision analysis for Compass satellite clock prediction based on a universal clock offset model. Scientia Sinica Phys Mech Atronomica 45 (2):079502-1-6
10. Xu x, Zhou y (2010) Research on high accuracy prediction model of earth orientation parameters. J Spacecraft TT&C Technol 29(2):70–76
11. Xu XQ, Zhou YH, Liao XH (2012) Short-term earth orientation parameters predictions by combination of the least-squares, AR model and Kalman filter. J Geodyn 62:83–86
12. Zhang Q, Wang Y, Sun Y (2015) Performance analysis of atomic clocks on board BDS/GPS/GLONASS Satellites. Hydrographic Surveying Charting 35(2):62–67
13. Zhu L, Li C, Liu L (2009) Research on methods for prediction clock error based on domestic hydrogen atomic clock. J Geodesy Geodyn 29(1):148–151

Relative Navigation for LEO Spacecraft Using Beidou-2 Regional Navigation System

Leizheng Shu and Wenbin Wang

Abstract LEO spacecraft relative navigation method based on Beidou measurement is researched. A series of tri-frequency combinations have been investigated with the purpose to improve the success rate of double-difference carrier phase ambiguity fixing and relative navigation accuracy. The process algorithms for two kinds of approaches, the kinematic relative navigation approach, and dynamic relative navigation approach, are investigated. The ambiguity fixing performance and relative navigation accuracy are validated using the simulated Beidou-2 regional navigation system scenario. The results showed that the single frequency and wide-lane combination ambiguity fixed rate drops rapidly with increasing baseline length, but S0 ultra-wide-lane combination ambiguity can be 100 % accurately resolved under three different baseline lengths. Concern the relative navigation accuracy, single frequency carrier phase especially B1 carrier phase relative positioning accuracy is highest for short baseline. With the increase of baseline length, the advantage of Beidou multi-frequency ionospheric-free combination gradually revealed: when the baseline length increased to 220 km, the relative positioning accuracy of ionospheric-free combination can increase by 75 % at most.

Keywords Beidou-2 regional navigation system · LEO spacecraft · Relative navigation · Tri-frequency combination · Ambiguity fixing

L. Shu (✉) · W. Wang
Key Laboratory of Space Utilization, Technology and Engineering Center for Space Utilization, Chinese Academy of Sciences, Beijing 100094, China
e-mail: shuleizheng@csu.ac.cn

W. Wang
e-mail: wangwenbin@csu.ac.cn

J. Sun et al. (eds.), *China Satellite Navigation Conference (CSNC) 2016 Proceedings: Volume III*, Lecture Notes in Electrical Engineering 390,
DOI 10.1007/978-981-10-0940-2_4

1 Introduction

GNSS-based spacecraft relative navigation is one of the most important technologies for on-orbit service and formation flying missions. At present, most of the in-orbit LEO spacecraft relative navigation depends on the GPS system. 1998, Japan's space agency (NASDA) demonstrated the GPS-based relative navigation technology for the first time in the ETS-VII mission [1]. German DLR and NASA launched the GRACE (Gravity Recovery and Climate Experiment) mission in 2002, which turns out to be the representation of the relative navigation research, see [2]. Kores et el. [3] adopted the dual-frequency GPS P code pseudorange and carrier phase observations in the reduced dynamic EKF filter to achieve the mm and mu m/s level of accuracy for relative position and velocity, respectively. In recent years, the successful in-orbit implementation of GPS-based relative navigation technology includes: Orbital Express [4] in 2007, PRISMA [5], and TanDEM-X/TerraSAR-X [6] in 2010. In October 2012, China's SJ-9 (Shi Jian-9 Formation Flight Mission) technology demonstration satellites were launched to perform the high precision GPS baseline measurement test [7].

China has launched the plan to expand its Beidou navigation system from the regional operation to global navigation system [8]. To research spacecraft relative navigation technology based on Beidou system is of great significance to improve the accuracy of orbit relative navigation, to enhance the safety of China's space mission autonomy and to extend the application of Beidou in space. Two kinds of Beidou-based LEO spacecraft relative navigation approaches, the kinematic relative navigation approach and dynamic relative navigation approach, are investigated in this article. A series of tri-frequency combinations have been investigated with the purpose to improve the success rate of double-difference carrier phase ambiguity fixing and relative navigation accuracy. The ambiguity fixing performance and relative navigation accuracy are validated using the simulated scenario.

2 Beidou Satellite System and Observation

2.1 Beidou Satellite

The Chinese Beidou navigation system is being gradually perfected in construction. A constellation composed of five geostationary Earth orbit (GEO) satellites, five inclined geosynchronous orbit (IGSO) satellites, and four Medium Earth orbit (MEO) satellites has been deployed by 2012 for providing regional navigation service.

By the end of 2020, China will complete the Beidou navigation satellite constellation, which consists of five GEO, three IGSO, and 27 MEO satellites. The MEO satellites will offer complete global coverage, similar to the GPS and GLONASS.

The IGSO and GEO satellites will improve the visibility and availability for users in China and neighboring regions. The GEO satellites are operating in orbit at an altitude of 35,786 km and positioned at 58.75°E, 80°E, 110.5°E, 140°E, and 160°E, respectively. The MEO satellites are operating in orbit at an altitude of 21,528 km and an inclination of 55° to the equatorial plane. The IGSO satellites are operating in orbit at an altitude of 35,786 km and an inclination of 55° to the equatorial plane [8].

2.2 Beidou Tri-frequency Observation

Beidou system provides three frequency signal, namely, B1, B2, and B3. Taking consideration of the following double-differenced carrier phase measurement equation:

$$\phi_i[m] = \rho + \lambda_i N_i - \left(\frac{f_1}{f_i}\right)^2 I_1 \tag{1}$$

where ϕ_i is the double-differenced phase measurement in meters; ρ is the double-differenced geometrical term which indicates the geometrical distance between receiver and Beidou satellite; λ_i is the wavelength in meters; N_i is the integer ambiguity; I_1 is the ionospheric delay on B1 in meters; and i is the frequency index.

For any integer coefficients i_1, i_2, and i_3, the linear combination which preserves the integer nature of the ambiguities is denoted as:

$$\varphi[cy] = i_1\varphi_1[cy] + i_2\varphi_2[cy] + i_3\varphi_3[cy] \tag{2}$$

By substituting Eq. (1) into Eq. (2) with consideration of the relation: $\phi_i\,[cy] = \phi_i\,[m]/\lambda_i$, one can show that this combination expressed in cycles:

$$\begin{aligned}\varphi[cy] = \rho \Big/ & \frac{1}{\frac{i_1}{\lambda_1} + \frac{i_2}{\lambda_2} + \frac{i_3}{\lambda_3}} + (i_1N_1 + i_2N_2 + i_3N_3) \\ & - \left(\frac{i_1\lambda_1 + i_2\lambda_2 + i_3\lambda_3}{\lambda_1^2}\right) I_1\end{aligned} \tag{3}$$

The resulting integer ambiguity $N = N(i_1, i_2, i_3)$, and the frequency $f = f(i_1, i_2, i_3)$ of this combination correspond to:

$$N(i_1, i_2, i_3) = i_1N_1 + i_2N_2 + i_3N_3 \tag{4}$$

$$f(i_1, i_2, i_3) = i_1f_1 + i_2f_2 + i_3f_3 = f_0(i_1k_1 + i_2k_2 + i_3k_3) \tag{5}$$

According to Cocard's definition, see [9], $k = i_1k_1 + i_2k_2 + i_3k_3$ is called the lane number, which uniquely defines the wavelength of every combination, regardless of any other properties of that combination. For Beidou system, k_1=763, k_2=620, k_3=590, corresponding to the frequency of B1, B3, and B2, respectively. The combination wavelength can be written as:

$$\lambda(i_1, i_2, i_3) = c/kf_0 \tag{6}$$

where base frequency f_0 = 2.046 MHz. We define the wide-lane combination as the resulting wavelength larger than the largest of the three base wavelengths, among which the ultra-wide-lane combinations are those with resulting wavelength larger than 2.93 m; the narrow-lane combinations are those with the resulting wavelength smaller than the smallest base wavelength.

If we assume that the noise on all three frequencies expressed in cycles is the same for all the phase measurements, a noise amplification factor n, with respect to cycles, corresponding to

$$n = \sqrt{i_1^2 + i_2^2 + i_3^2} \tag{7}$$

Taking the first-order ionospheric delay to be inversely proportional to the square of the frequency, we can derive the ionospheric delay amplification factor with respect to B1, q (in units of cycle), and κ (in units of meter) as:

$$q = \frac{1}{\lambda_1}(i_1\lambda_1 + i_2\lambda_2 + i_3\lambda_3) \tag{8}$$

$$\kappa(i_1, i_2, i_3) = \left(\frac{i_1\lambda_1 + i_2\lambda_2 + i_3\lambda_3}{\lambda_1^2}\right) \cdot \lambda(i_1, i_2, i_3) \tag{9}$$

Table 1 summarizes potentially interesting combinations and their relevant features. We regrouped all the possible combinations based on the sum s of i_1, i_2, and i_3.

An investigation of Table 1 leads to the following conclusions:

1. S0 region collects wide-lane and ultra-wide-lane combinations, which corresponds to large wavelength with a low ionospheric sensitivity.
2. S1*a* includes the combinations with the coefficient sum of 1 and small lane number. In this region, the wavelength is larger than 2.93 m, but the ionospheric amplification factor is about 2.3 with respect to cycles. If one considers the amplification factor κ with respect to meters, one obtains huge values since the wavelengths are large in this region.
3. S1*b* includes the combinations with the coefficient sum of 1 and large lane number. In this region, the wavelengths are about 10–12 cm, but they are insensitive to the ionosphere.

Table 1 Feature statistics of Beidou tri-frequency combination

Region	k	(i_1, i_2, i_3)	$\lambda(m)$	n	q	κ
S0	23	(1, −5, 4)	6.3707	6.4807	0.0197	0.6535
	30	(0, 1, −1)	4.8842	1.4142	−0.0626	−1.5921
	43	(1, −4, 3)	2.7646	5.0990	−0.0429	−0.6176
	143	(1, −1, 0)	1.0247	1.4142	−0.2306	−1.2304
	173	(1, 0, −1)	0.8470	1.4142	−0.2932	−1.2931
S1*a*	2	(−6, 15, −8)	73.2631	18.0278	2.1139	806.4319
	11	(−3, −2, 6)	13.3206	7	2.2980	159.3939
	18	(−4, 4, 1)	8.1403	5.7446	2.2158	93.9224
	41	(−3, −1, 5)	3.5738	5.9161	2.2355	41.6009
	48	(−3, −1, 5)	3.0526	6.4031	2.1532	34.2257
S1*b*	1252	(4, −1, −2)	0.1170	4.5826	0.1829	0.1114
	1282	(4, 0, −3)	0.1143	5	0.1203	0.0716
	1312	(4, 1, −4)	0.1117	5.7446	0.0578	0.0336
	1425	(5, −1, −3)	0.1028	5.9161	−0.1103	−0.0590
	1455	(5, 0, −4)	0.1007	6.4031	−0.1729	−0.0907

3 LEO Spacecraft Relative Navigation

Generally there are two kinds of method to implement the carrier differenced Beidou-based relative navigation: kinematic approach and (reduced) dynamic approach.

3.1 Recursive Least-Squares Kinematic Approach

The kinematic approach does not involve any satellite force models at all, and epoch-by-epoch relative positions are computed in purely kinematic mode by processing differential Beidou carrier phase measurements as the main observables.

The kinematic approach mainly implements least squares (LSQ) estimator to solve the ambiguity and the relative position parameters. Least square method can solve the single epoch ambiguity float solution and its covariance matrix, and then employ the LAMBDA method (see [10]) to search for integer solutions. But experiment results show that the single epoch ambiguity fixing success rate is not high, especially when observation noise is high and baseline length is large.

It should be noted that the ambiguities vector is constant in the absence of cycle slips or satellites setting and rising, thus it is possible to obtain a much improved float solution by carrying information from one epoch to the consecutive one. To implement this, a recursive LSQ estimator is developed to process the ambiguity estimate sequentially one epoch at a time. Figure 1 illustrates the algorithm flow

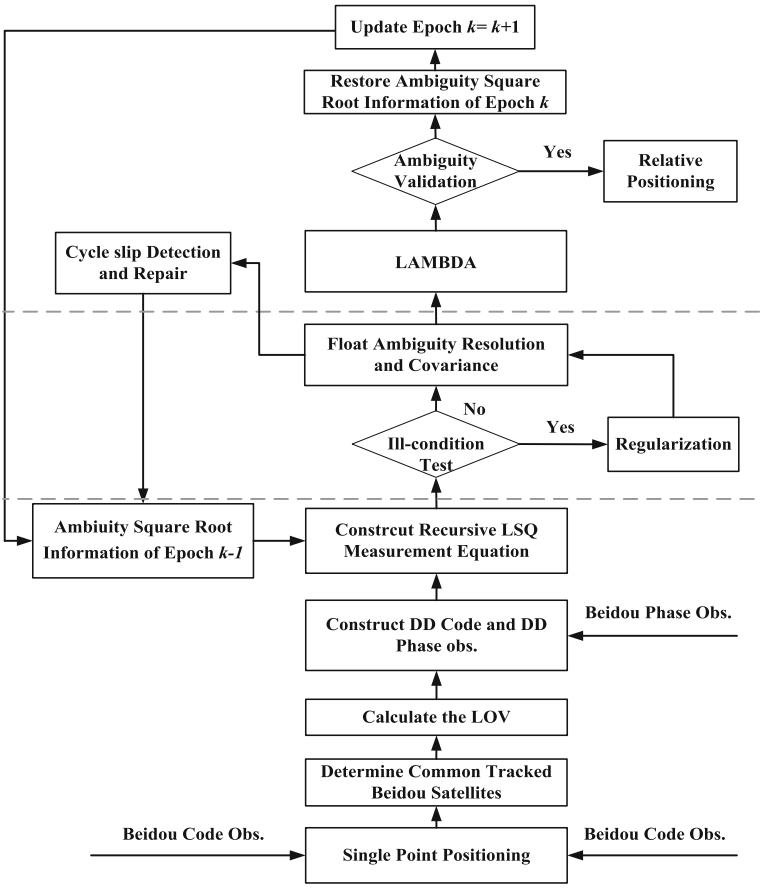

Fig. 1 Algorithm flow chart of the recursive LSQ procedure

chart of the recursive LSQ procedure: a posteriori ambiguity float solution at the previous epoch is exploited as a pseudo-measurement and passed forward to the functional model of the current epoch for improving the float estimates.

3.2 Reduced Dynamic Approach

The basic principle of reduced dynamic approach is: the spacecraft relative dynamic model is first used to calculate a reference relative orbit, and then the high precision Beidou observation is employed to correct the reference relative orbit, results in an optimal estimation of the relative state [11].

Figure 2 shows a conceptual flow chart of the filtering scheme. The Beidou relative navigation filter is implemented in four steps: the time update, the tracked

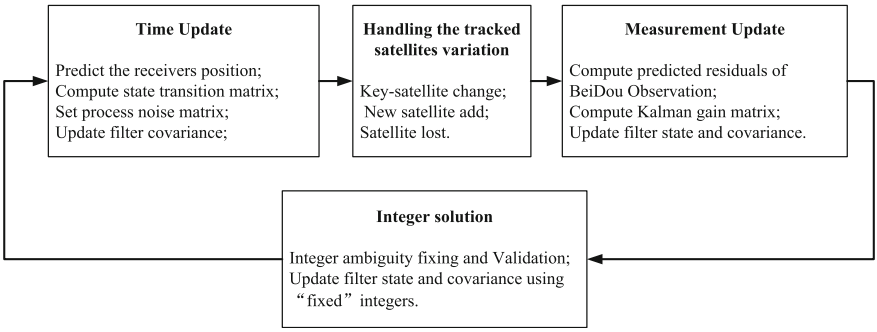

Fig. 2 Algorithm flow chart of the reduced dynamic procedure

satellites variation handling, the measurement update, and the integer solution. Reduced dynamic filter also estimates other parameters at the same time, such as ionospheric delay error, receiver clock error, and empirical acceleration parameter, to improve the fitting degree between the dynamic reference orbit and Beidou observed data.

Therefore the ambiguity float solution solved from the reduced dynamics approach is convergence faster, and the navigation results are smoother at the same time.

4 Simulation and Results

4.1 Simulation Scenario Settings

Simulated scenario is built to test the LEO spacecraft relative navigation performance of Beidou-2 regional navigation system. The Beidou constellation, consists of five GEO, five IGSO, and four MEO satellites, is set up according to the existing 14 satellites' orbit parameters. Figure 3 illustrates the sub-satellite points of the simulated constellation.

Formation spacecraft circles on the GRACE-type orbit, with the orbital inclination of 89° and radius of 6847.75 km. Three groups of simulation are carried out, with baseline length between formation satellites set to 10, 100, and 100 km, respectively. The rest simulation settings can be found in Table 2.

The Beidou satellites visible duration for the first formation spacecraft is given in Fig. 4. It can be seen that frequent tracked satellite variation occurred during 5 h simulation. Due to the less number of Beidou-2 regional navigation system, and the concentration distribution over the Asia-Pacific region, so only when the two spacecraft formation through the Asia-Pacific region can they synchronously observe more than five Beidou satellites. We only investigate the relative navigation performance during this region.

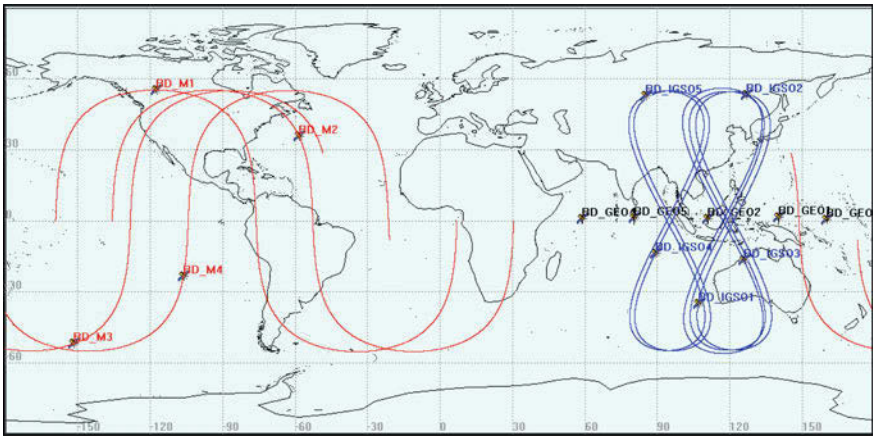

Fig. 3 Sub-satellite points of Beidou-2 regional navigation system

Table 2 The simulation scenario settings

Class	Parameter settings
Beidou constellation	5GEO + 5IGSO + 4MEO
Formation spacecraft	GRACE-type orbit ($i \approx 89°$, r = 6847.75 km) baseline length = 10, 100 and 220 km
Simulation duration	5 h
Simulation step size	1 s
Ionospheric model	CIM(China Ionospheric Model) the ionospheric delay for B1/B2/B3 is inversely proportional to the square of the corresponding frequency
Ambiguity	Fixing integer
Measurement noise	the code noise for B1/B2/B3 is set to 1 times the corresponding carrier wavelength; the phase noise for B1/B2/B3 is set to 0.025 times the corresponding carrier wavelength

4.2 Ambiguity Resolution Performance

The ambiguity resolution is investigated for S0 ultra-wide-lane combination (1, −5, 4), (0, 1, −1), and (1, −4, 3), S0 most used wide-lane combination (1, −1, 0), S1*a* ultra-wide-lane combination (−4, 4, 1) and B1 (1, 0, 0). Tables 3, 4, and 5 summarize the ambiguity success rate for three different methods: recursive LSQ kinematic method, reduced dynamic method, and the famous tri-frequency carrier phase ambiguity resolution method-TCAR.

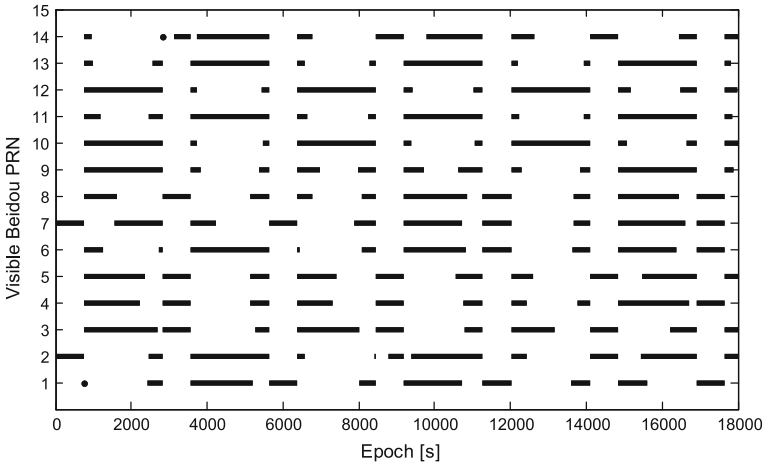

Fig. 4 The Beidou satellites visible duration

Table 3 Ambiguity success rate for recursive LSQ kinematic method

Baseline length	(1, −5, 4)	(0, 1, −1)	(1, −4, 3)	(1, −1, 0)	(−4, 4, 1)	(1, 0, 0)
10 km	100 %	100 %	100 %	100 %	100 %	100 %
100 km	100 %	100 %	100 %	100 %	99.4 %	99.4 %
220 km	100 %	100 %	100 %	100 %	60.97 %	60.88 %

Table 4 Ambiguity success rate for reduced dynamic method

Baseline length	(1, −5, 4)	(0, 1, −1)	(1, −4, 3)	(1, −1, 0)	(−4, 4, 1)	(1, 0, 0)
10 km	100 %	100 %	100 %	100 %	100 %	100 %
100 km	100 %	100 %	100 %	100 %	100 %	100 %
220 km	100 %	100 %	100 %	100 %	100 %	96.21 %

Table 5 Ambiguity success rate for TCAR method

Baseline length	(1, −5, 4)	(0, 1, −1)	(1, −4, 3)	(1, −1, 0)	(−4, 4, 1)	(1, 0, 0)
10 km	100 %	100 %	100 %	100 %	100 %	24.06 %
100 km	100 %	100 %	100 %	97.23 %	89.84 %	12.20 %
220 km	100 %	100 %	100 %	97.01 %	38.89 %	7.14 %

An analysis of Tables 3, 4 and 5 leads to the following conclusions:

1. S0 region ultra-wide-lane ambiguity can be accurately fixed under three different baseline length.
2. S1*a* ultra-wide-lane combination (−4, 4, 1) ambiguity can be 100 % fixed only under reduced dynamic method. The recursive LSQ kinematic method gets

worse success rate while the TCAR gets the worst. This is because even though the wavelength is large for this combination, the ionospheric amplification factor is magnificent. The reduced dynamic method can ensure the ambiguity convergence accurately because we use dynamics parameters to absorb those systemic error.

3. The B1 ambiguity fixing is challenging under long baseline. Even using the orbital dynamics information, the reduced dynamic method can only obtain B1 ambiguity success rate to 96.21 % under the baseline length 220 km.

4.3 Relative Positioning Precision

Figure 5 demonstrates the deviation of relative positioning using only B1 phase for the first 1500 s. Table 6 lists the corresponding ENU deviation statistics for 5 h.

Combined with Fig. 5 and Table 6, we can see that Beidou B1 relative positioning error increases with the increase of baseline length; Consider the ENU deviation, the East accuracy is always better than the North and Up direction. This

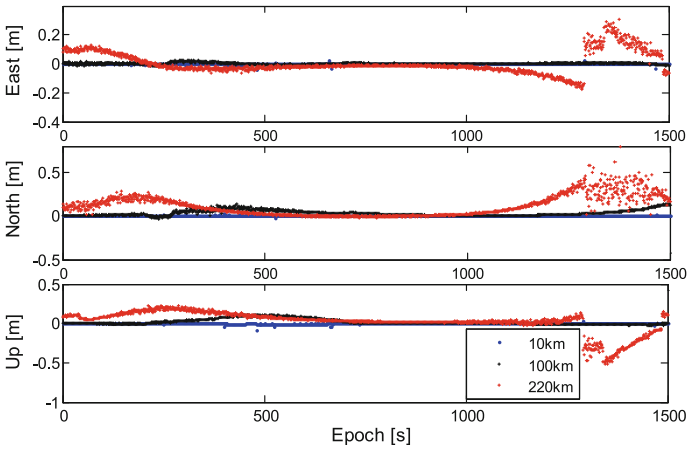

Fig. 5 The deviation of relative positioning using only B1 carrier phase (the first 1500 s)

Table 6 ENU deviation statistics for relative positioning using only B1 carrier phase (5 h)

Baseline length (km)	Mean (mm)			Std (mm)		
	East	North	Up	East	North	Up
10	−0.89	2.02	−1.30	5.05	3.86	6.47
100	1.88	32.14	17.69	5.99	31.52	35.01
220	5.68	109.69	18.58	74.19	113.93	131.21

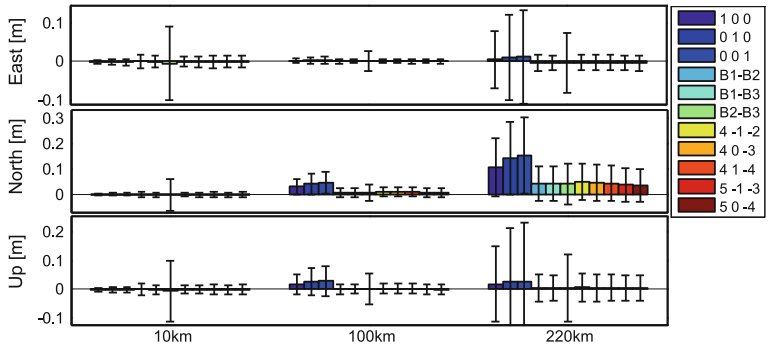

Fig. 6 The deviation of relative positioning using combine measurement (5 h)

can be explained from the Beidou observation geometry: when the formation flies across the Asia-Pacific region, the deployed GEO satellite increases the constraints on East–West direction.

Figure 6 summarizes the relative positioning deviations using different combinations observation. For each baseline length, the first three groups utilize the B1, B3, and B2 single frequency, group 4–6 are three ionospheric-free combinations, group 7–11 are narrow-lane combinations with repressive ionospheric chosen from S1*b* region. The results show that the relative positioning precision is higher using Beidou single frequency carrier phase, especially B1, under the condition of short baseline. With the increase of baseline length, the advantage of Beidou tri-frequency ionosphere-free/repressive combination gradually increases. When the baseline length increased to 220 km, the relative positioning accuracy of ionospheric-free combination can increase by 75 % at most.

5 Summary

A series of tri-frequency combinations have been investigated with the purpose to improve the success rate of double-difference carrier phase ambiguity fixing and relative navigation accuracy. The ambiguity fixing performance and relative navigation accuracy for Beidou-based LEO formation spacecraft are validated using the simulated scenario. The results reveal a variety of optional observation combinations which can be offered by Beidou system under different navigation algorithms and for different baseline length. Future work includes research in Beidou-based high dynamic attitude determination and positioning technology, as well as relative navigation algorithm based on multiple navigation system.

Acknowledgments This study is funded by the ‘Breeding Project’ of Innovation Academy, Chinese Academy of Sciences.

References

1. Mokuno M, Kawano I, Kasai T (1999) Experimental results of autonomous rendezvous docking on Japanese ETS-VII satellite. Guid Control 1999(101):P221–P238
2. Jaeggi A et al (2007) Precise orbit determination for GRACE using undifferenced or doubly differenced GPS data. Adv Space Res 39(10):P1612–P1619
3. Kroes R, Montenbruck O, Bertiger W et al (2005) Precise GRACE baseline determination using GPS. GPS Solutions 9(1):P21–P31
4. Weismuller TP, Leinz MR, Company TB (2006) GN&C technology demonstrated by the orbital express autonomous rendezvous and capture sensor system. American Astronautical Society guidance and control conference, Breckenridge, Co.
5. D'Amico S, Ardaens JS, Larsson R (2012) Spaceborne autonomous formation-flying experiment on the PRISMA mission. J Guid Control Dyn 35(3):P834–P850
6. Montenbruck O, Wermuth M, Kahle R (2011) GPS, based relative navigation for the TanDEM-X Mission—First flight results. Navig J Inst Navig 58(4):P293–P304
7. Chen P, Shu L, Ding R et al (2015) Kinematic single-frequency relative positioning for LEO formation flying mission. GPS Solutions 19(4):P525–P535
8. China Satellite Navigation Office (2013) BeiDou Navigation Satellite System Signal In Space Interface Control Document: Open Service Signal (Version 2.0)
9. Cocard M, Bourgon S, Kamali O et al (2008) A systematic investigation of optimal carrier-phase combinations for modernized triple-frequency GPS. J Geodesy 82(9):P555–P564
10. Teunissen PJG (1995) The least-squares ambiguity decorrelation adjustment: a method for fast GPS integer ambiguity estimation. J Geodesy 70(1–2):P65–P82
11. Wu SC, Yunck TP, Thornton CL (1991) Reduced-dynamic technique for precise orbit determination of low Earth satellites. J Guid Control Dyn 14(1):P24–P30

Analysis on Energy System Safety in GEO Satellite Complex Eclipse

Jinfei Chen, Xingyu Wang, Tao Wang and Ting Wang

Abstract The energy system is one of the key systems of satellite. Once the energy system fails, it can easily lead to failure of other systems. Therefore, the energy system safety is crucial to the satellite in orbit. For GEO satellites, the eclipse is a common astronomical phenomenon. When the satellite is in eclipse, due to the Earth or the Moon blocking the Sun, the energy of solar array will decline, the battery will discharge, and the operation mode of energy system will change. Especially, "*complex eclipse*", which is generated by the continuous alternate block of the Earth and the Moon, will bring the worse influence of satellite energy supply, easily leading to failure of satellite. Therefore, to analyze the impact of complex eclipse to the energy system, safety is quite necessary. First, this paper describes the principles of complex eclipse, GEO satellite energy system and the influence to the energy system caused by the complex eclipse, furthermore determines the relationship between eclipse and the operation mode of energy system, analyzes the energy system safety in GEO satellite complex eclipse, establishes the reasonable disposal strategy based on the result, and applies it. The conclusions show that, the eclipse does affect the energy system of GEO satellite; the method given by this paper is to ensure the energy system safety in GEO satellite complex eclipse with practical value.

Keywords GEO satellite · Eclipse · Energy system safety · Disposal strategy

J. Chen (✉)
Key Laboratory for Fault Diagnosis and Maintenance of Spacecraft in Orbit,
710043 Xi'an, China
e-mail: chen2jin3fei1@163.com

X. Wang · T. Wang · T. Wang
Xi'an Satellite Control Center, 710043 Xi'an, China
e-mail: wxyyx_001@sina.com

T. Wang
e-mail: wang1tao1@163.com

T. Wang
e-mail: wang2ting2@163.com

J. Sun et al. (eds.), *China Satellite Navigation Conference (CSNC) 2016 Proceedings: Volume III*, Lecture Notes in Electrical Engineering 390,
DOI 10.1007/978-981-10-0940-2_5

1 Introduction

Energy System is one of the core critical systems of satellite, which is mainly constituted by a number of hardware components such as the power produce, power storage, power control, voltage transformation, supply distribution, etc. A large number of fault cases statistical results showed that: the failure of GEO satellites in orbit occurred, the energy system failures account for a large proportion. Especially in the eclipse, due to the effect of the Earth or the Moon obscured the sun for solar array, there is not sufficient power to provide, the battery must discharge to replenish the energy satellite required. When the satellite desired energy consumption exceeds the stored battery power, it will lead to serious consequences that the whole satellite lacks of power, which fails easily. It is quite essential to make an accurate estimate of energy consumption required in eclipse for satellite, to take the necessary avoidance strategy against dangerous situations that may occur [1]. Aiming to a bad case that eclipse shadow caused by the combined effect of the Earth and the Moon, this paper proposed a method of GEO satellite energy system analysis, which can not only predict eclipses occlusion, but also estimate the eclipse of satellite energy consumption. At present, the method has been applied in the actual management of GEO satellite.

2 Fundamental

2.1 Principle and Calculation Model of Eclipse

Eclipse is a kind of astronomical phenomena which is occurred when the Moon or the Earth blocks sunshine to the satellite. Eclipse includes two cases which depend on the blocker is the Earth or the Moon. The Earth eclipse generates because the Earth blocks the sunshine, it took place in spring and autumn every year fixedly, the time span is usually 23 days around the vernal equinox or the autumnal equinox, so the Earth eclipse lasts about 92 days each year. The principle of the Moon eclipse is similar to the Earth eclipse, it generates because the Moon blocks the sunshine. Compared with the Earth eclipse, there is no law of the Moon eclipse. That is because the Moon eclipse is the result of Earth–-Sun revolution, Moon–Earth revolution, and the Earth rotation combined effect. Generally speaking, the Moon eclipse often occurs around the first day of lunar month [2].

One single eclipse process generally contains three stages “penumbra—umbra—penumbra”, uses method based on space visual field to calculate eclipses commonly, which sets the spatial position of the satellite as a reference point of the visual field, by calculating the relative visual angle of the Sun, the Earth, and the Moon to the reference point, to achieve the calculation of eclipse time, eclipse phase [3].

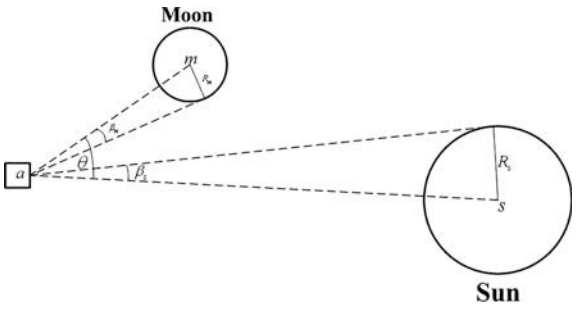

Fig. 1 Principle of eclipse

Take the Moon as the blocker in the discussion of the eclipse's principle, in the J2000 coordinate system as shown in Fig. 1, the position vector of the satellite is $\mathbf{r}_a = [X_a \quad Y_a \quad Z_a]^T$, the position vector of the Sun is $\mathbf{r}_s = [X_s \quad Y_s \quad Z_s]^T$, the position vector of the Moon is $\mathbf{r}_m = [X_m \quad Y_m \quad Z_m]^T$. Therefore

$$\begin{cases} \overrightarrow{as} = \mathbf{r}_s - \mathbf{r}_a = \begin{bmatrix} X_s - X_a \\ Y_s - Y_a \\ Z_s - Z_a \end{bmatrix} \\ \overrightarrow{am} = \mathbf{r}_m - \mathbf{r}_a = \begin{bmatrix} X_m - X_a \\ Y_m - Y_a \\ Z_m - Z_a \end{bmatrix} \end{cases} \tag{1}$$

The visual radius of the Sun is R_s, the visual radius of the Moon is R_m. The visual half field angle of satellite to the Sun is β_s, the visual half field angle of satellite to the Moon is β_m. Therefore

$$\begin{cases} \beta_s = \arcsin\left(\dfrac{R_s}{\sqrt{(X_s - X_a)^2 + (Y_s - Y_a)^2 + (Z_s - Z_a)^2}}\right) \\ \beta_m = \arcsin\left(\dfrac{R_m}{\sqrt{(X_m - X_a)^2 + (Y_m - Y_a)^2 + (Z_m - Z_a)^2}}\right) \end{cases} \tag{2}$$

defines the space angle between vector $\overrightarrow{as}$ and vector $\overrightarrow{am}$ which is θ, therefore

$$\theta = \arccos\left(\frac{\overrightarrow{as} \cdot \overrightarrow{am}}{\left|\overrightarrow{as}\right| \cdot \left|\overrightarrow{am}\right|}\right) \tag{3}$$

So that summarized the judgment basis of the Moon eclipse:

1. When $\theta \geq \beta_s + \beta_m$, there is no eclipse;
2. When $|\beta_s - \beta_m| \leq \theta < \beta_s + \beta_m$, there is penumbra;
3. When $\theta < |\beta_s - \beta_m|$, there is umbra.

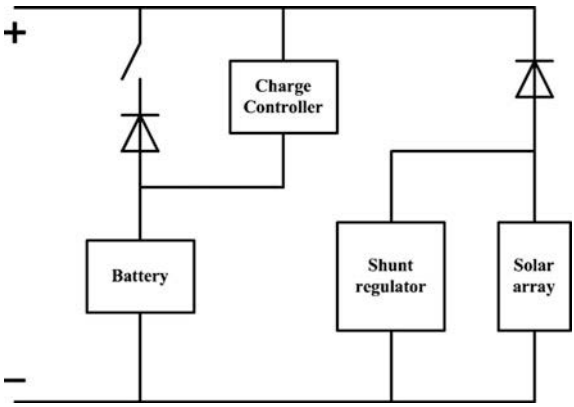

Fig. 2 Structure of GEO satellite energy system

2.2 Introduction of GEO Satellite Energy System

Currently, the vast majority GEO satellites in orbit are designed using the solar array and the batteries as the energy supply.

Figure 2 shows that, GEO satellite energy system consists of solar array, battery, shunt regulator, and charge controller. According to its design, the solar array provides energy to the satellite payload, charges the battery at the same time in illumination. The battery provides energy to the satellite payload in eclipse.

As the input source, the array is exposed to the cosmic vacuum environment, its output could be effected by the incident light intensity, ambient temperature, load power, etc., [4] so that it would lead to a certain amplitude fluctuation. In order to adapt to and regulate the illumination, the shunt regulator is designed to handle the excessive power of solar array. In the illumination, when the solar array output power is greater than satellite payload power consumption, the excessive power is used to replenish the battery; the shunt regulator here is regulating the battery charging current. In the eclipse, the output of solar array decreases because of the block, the shunt current also decreases. When the shunt current drops to zero, which represents the solar array's energy output which is not sufficient to support the satellite, the battery starts to provide energy to the satellite under the control of charge controller.

2.3 The Impact of Eclipse to the Energy System

It is easy to summarize from the above analysis that, there will be two cases of satellite energy supply in eclipse as following: one is the eclipse does not lead shunt current to decrease to zero, in which case the satellite solar array will continue to be used as energy supply, battery does not discharge; the other is the eclipse which

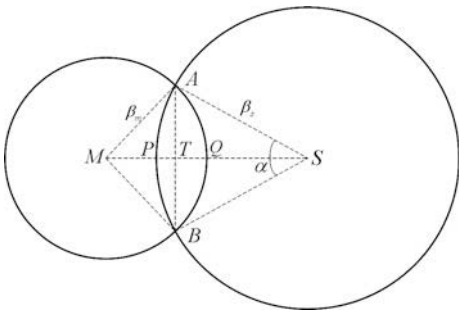

Fig. 3 Model of the Moon eclipse

does lead shunt current to decrease to zero, in which case the satellite will start to use battery as an energy supplement reinforcement, the battery discharges.

Apparently, there is a certain relationship between blocked area and the energy supply mode switch. Therefore, a reasonable solution is to start form the blocked area in eclipse, establish the relationship between blocked area and the energy supply mode switch, so that to forecast the mode switch of energy supply [5, 6].

The model of Moon eclipse shown in Fig. 3 is the example to discuss. The block area W is surrounded by the arc $\overset{\frown}{APB}$ and arc $\overset{\frown}{AQB}$, the area is divided into two parts by the string $\overline{AB}$: one is W_1, surrounded by arc $\overset{\frown}{APB}$ and string $\overline{AB}$; the other is W_2, surrounded by arc $\overset{\frown}{AQB}$, and string $\overline{AB}$. Make the area of sector $APBS$ as W_{APBS}, the area of triangle ABS is W_{ABS}, the central angle is α.

Segment MS is a short arc of circle, which passes through the center of Sun and Moon, takes the satellite as center. As θ is a little angle, it can be approximated as $\overline{AB} \approx \overset{\frown}{MS} = \theta$, the length of arc and string is equal.

According to the law of cosines, in triangle ΔABS

$$\cos\frac{\alpha}{2} = \frac{\beta_s^2 + \theta^2 - \beta_m^2}{2\beta_s\theta} \tag{4}$$

in triangle ΔATS

$$\cos\frac{\alpha}{2} = \frac{TS}{\beta_s} \tag{5}$$

according to the simultaneous equation

$$TS = \frac{\beta_s^2 + \theta^2 - \beta_m^2}{2\theta} \tag{6}$$

so

$$\begin{cases} W_{APBS} = \frac{1}{2}\alpha\beta_s^2 = \arccos\left(\frac{TS}{\beta_s}\right)\beta_s^2 \\ W_{ABS} = \frac{1}{2}\overline{AB} \times \overline{TS} = TS\sqrt{\beta_S^2 - TS^2} \\ W_1 = \arccos\left(\frac{TS}{\beta_s}\right)\beta_s^2 - TS\sqrt{\beta_s^2 - TS^2} \end{cases} \tag{7}$$

similarly

$$W_2 = \arccos\left(\frac{\theta - TS}{\beta_m}\right)\beta_m^2 - (\theta - TS)\sqrt{\beta_s^2 - TS^2} \tag{8}$$

so that the block area is

$$\begin{aligned} W &= W_1 + W_2 \\ &= \arccos\left(\frac{TS}{\beta_s}\right)\beta_s^2 - TS\sqrt{\beta_s^2 - TS^2} \\ &\quad + \arccos\left(\frac{\theta - TS}{\beta_m}\right)\beta_m^2 - (\theta - TS)\sqrt{\beta_s^2 - TS^2} \\ &= \arccos\left(\frac{TS}{\beta_s}\right)\beta_s^2 + \arccos\left(\frac{\theta - TS}{\beta_m}\right)\beta_m^2 - \theta\sqrt{\beta_s^2 - TS^2} \end{aligned} \tag{9}$$

brings formula (6) in

$$\begin{aligned} W = &\arccos\left(\frac{\beta_s^2 + \theta^2 - \beta_m^2}{2\theta\beta_s}\right)\beta_s^2 + \arccos\left(\frac{\beta_m^2 + \theta^2 - \beta_s^2}{2\theta\beta_m}\right)\beta_m^2 \\ &- \theta\sqrt{\beta_s^2 - \left(\frac{\beta_s^2 + \theta^2 - \beta_m^2}{2\theta}\right)^2} \end{aligned} \tag{10}$$

When the satellite in illumination, the energy is provided by the solar array, the battery does not discharged. Suppose the load current of satellite is I_1, the shunt current is I_2, the total current which is outputted by solar array is $I = I_1 + I_2$. When the satellite is in eclipse, the total current decreases to I', which is

$$I' = I\left(1 - \frac{W}{\pi\beta_s^2}\right) \tag{11}$$

Make $\varepsilon = \frac{W}{\pi\beta_s^2}$, the relationship between blocked area and the energy supply mode switch is established:

1. When $I' \geq I_1$, which is $\left(1 + \frac{I_2}{I_1}\right)(1 - \varepsilon) \geq 1$, the battery does not discharge, the mode of energy system does not switch;
2. When $I' < I_1$, which is $\left(1 + \frac{I_2}{I_1}\right)(1 - \varepsilon) < 1$, the battery does discharge, the mode of energy system does switch.

3 Analysis of GEO Satellite Energy in Complex Eclipse

Before the autumn eclipse of a GEO satellite comes in 2015, use the above principle to analysis the energy system as following:

3.1 Eclipse Forecasts

Use the method based on space visual field to forecast autumn eclipse of the GEO satellite in 2015, the result shows that: the eclipse starts in Aug. 30th, ends in Oct. 16th, including three eclipse blocks caused by the Moon. Parts of the results are shown in Table 1.

3.2 Energy Analysis in Eclipse

To facilitate discussion, this paper only discussed in detail the status tail of north energy system in satellites, south part is similar.

Table 1 Parts of the result of eclipse forecast in 2015 autumn

Blocker	Start time	End time
The Earth	2015-08-30 02:37:12	2015-08-30 02:44:16
The Earth	2015-09-13 02:03:23	2015-09-13 03:08:45
The Moon	**2015-09-13 05:21:11**	**2015-09-13 06:03:10**
The Moon	**2015-09-13 14:03:23**	**2015-09-13 14:15:22**
The Earth	2015-10-13 02:10:01	2015-10-13 02:45:02
The Moon	**2015-10-13 17:31:17**	**2015-10-13 21:17:10**
The Earth	2015-10-14 02:12:48	2015-10-14 02:41:51
The Earth	2015-10-16 02:24:27	2015-10-16 02:29:38

3.2.1 Sep. 13th 05:21:11

1. Forecast the blocked area
   Using the orbit of Aug. 28th 2015, set a calculation point every two seconds, calculate the blocked area W, sketch $\varepsilon = \frac{W}{\pi\beta_s^2}$. The abscissa represents time, the ordinate represents the percentage of blocked area.
2. Establish an initial state of energy system
   As introduced in Sect. 2.1, the eclipse caused by the Earth is regular and repeatable. Using data mining algorithms, extract the telemetry parameters in every Spring and Autumn eclipse from 2013 to 2015, summarize the key parameter values of energy system to establish initial state of energy system in this eclipse.
3. Determine the discharging state of battery
   Since an initial state of energy system has been established, it is certain that $\frac{I_2}{I_1+I_2} \approx 27.8\,\%$. So, that when $\varepsilon = \frac{W}{\pi\beta_s^2} > \frac{I_2}{I_1+I_2} \approx 27.8\,\%$, the battery will discharge. As shown in Fig. 4, the shadow area is discharge capacity of battery. Calculate the area with integration, the discharge capacity of north battery is 2.325 A·h.
4. Forecast the battery's status
   This eclipse of the Moon starts about 2 h later since the last eclipse ends, it is a typical "complex eclipse". Since the battery would discharge, it is necessary to determine the battery's status before eclipse occurs. According to the managing files of this GEO satellite: if "North battery pressure 1" or "North battery pressure 2" is less than 4.9, it will be certain that the battery is not full. According to the value in Table 2, before the eclipse occurs, the capacity of battery has been charged approximately 85.4 %.
5. Conclusions of energy system
   Before the eclipse occurs, the battery is not fully charged, the capacity of battery is approximately 85.4 %. During the eclipse, the battery will discharge about 2.325 A·h. According to the managing files of this GEO satellite: the capacity of fully charged battery is 30 A·h, the warning percent of discharging is 73 %.

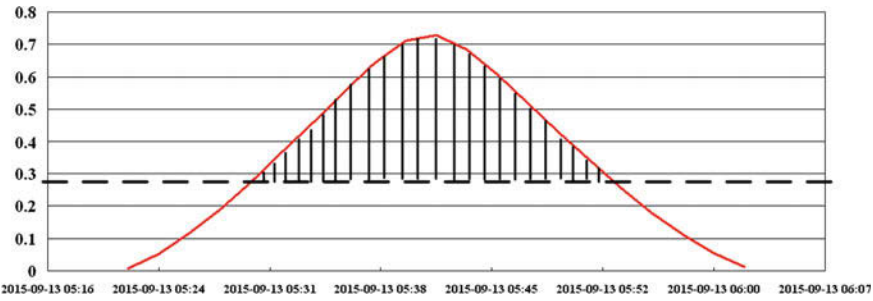

Fig. 4 Curve: the forecast proportion of block and discharge capacity in 05:21:11, 09-13-2015

Table 2 Initial state forecast of north energy system and battery

Parameter	Value	Parameter	Value
North main bus voltage	41.814	North battery voltage	38.784
North main bus load current	19.4025	North battery pressure 1(P1)	4.183
North shunt current	7.4852	North battery pressure 2(P2)	4.208

Table 3 Initial state forecast of north energy system

Parameter	Value
North main bus voltage	42.016
North main bus load current	21.105
North shunt current	12.693

In this eclipse, the battery will discharge about 9.1 %, which is far less than the warning percent, so the conclusion is energy system is safe, no need to take action.

3.2.2 Sep. 13th 14:03:23

1. Forecast the blocked area
2. Establish an initial state of energy system (Table 3)
3. Determine the discharging state of battery
   Since an initial state of energy system has been established, it is certain that $\frac{I_2}{I_1+I_2} \approx 37.6\,\%$. So that when $\varepsilon > 37.6\,\%$, the battery will discharge. As shown in Fig. 5, the largest percent of block is less than 0.8 %, which is far less than the switch value, so that the battery will not discharge at all.
4. Conclusions of energy system
   Since the battery will not discharge at all, the conclusion is energy system is safe, no need to take action.

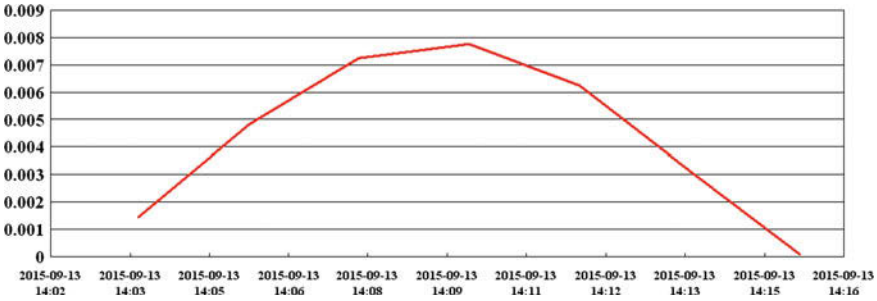

Fig. 5 Curve: the forecast proportion of block in 14:03:23, 09-13-2015

3.2.3 Oct. 13th 17:31:17

1. Forecast the blocked area
2. Establish an initial state of energy system
3. Determine the discharging state of battery
   Since an initial state of energy system has been established, it is certain that $\frac{I_2}{I_1+I_2} \approx 40.6\,\%$. So that when $\varepsilon > 40.6\,\%$, the battery will discharge. As shown in Fig. 6, the shadow area is discharge capacity of battery. Calculate the area with integration, the discharge capacity of north battery is 8.921 A·h.
4. Forecast the battery's status
   This eclipse of the Moon starts about 15 h later since the last eclipse ends, it is also a typical "complex eclipse". As shown in Table 4, before the eclipse occurs, the battery has been fully charged.
5. Conclusions of energy system
   Before the eclipse occurs, the battery is fully charged. During the eclipse, the battery will discharge about 8.921 A·h. In this eclipse, the battery will discharge about 29.7 %, which is less than the warning percent, so the conclusion is energy system is safe, no need to take action.

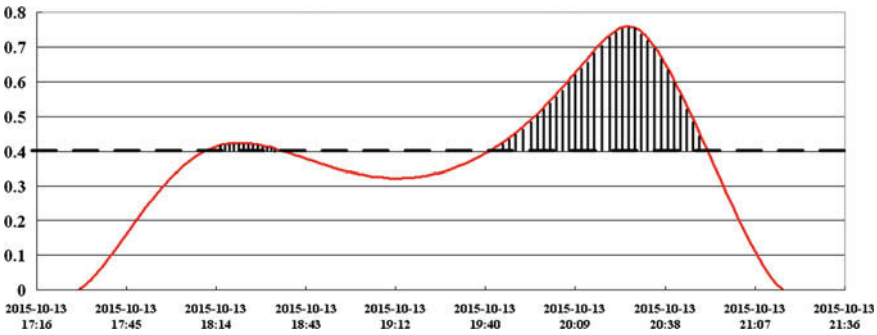

Fig. 6 Curve: the forecast proportion of block and discharge capacity in 17:31:17, 10-13-2015

Table 4 Initial state forecast of north energy system and battery

Parameter	Value	Parameter	Value
North main bus voltage	42.016	North battery voltage	38.986
North main bus load current	20.040	North battery pressure 1(P1)	4.980
North shunt current	13.669	North battery pressure 2(P2)	5.028